SOHO BECOMES BOGART:

Rescaling a Successful Mission to Support Living With a Star
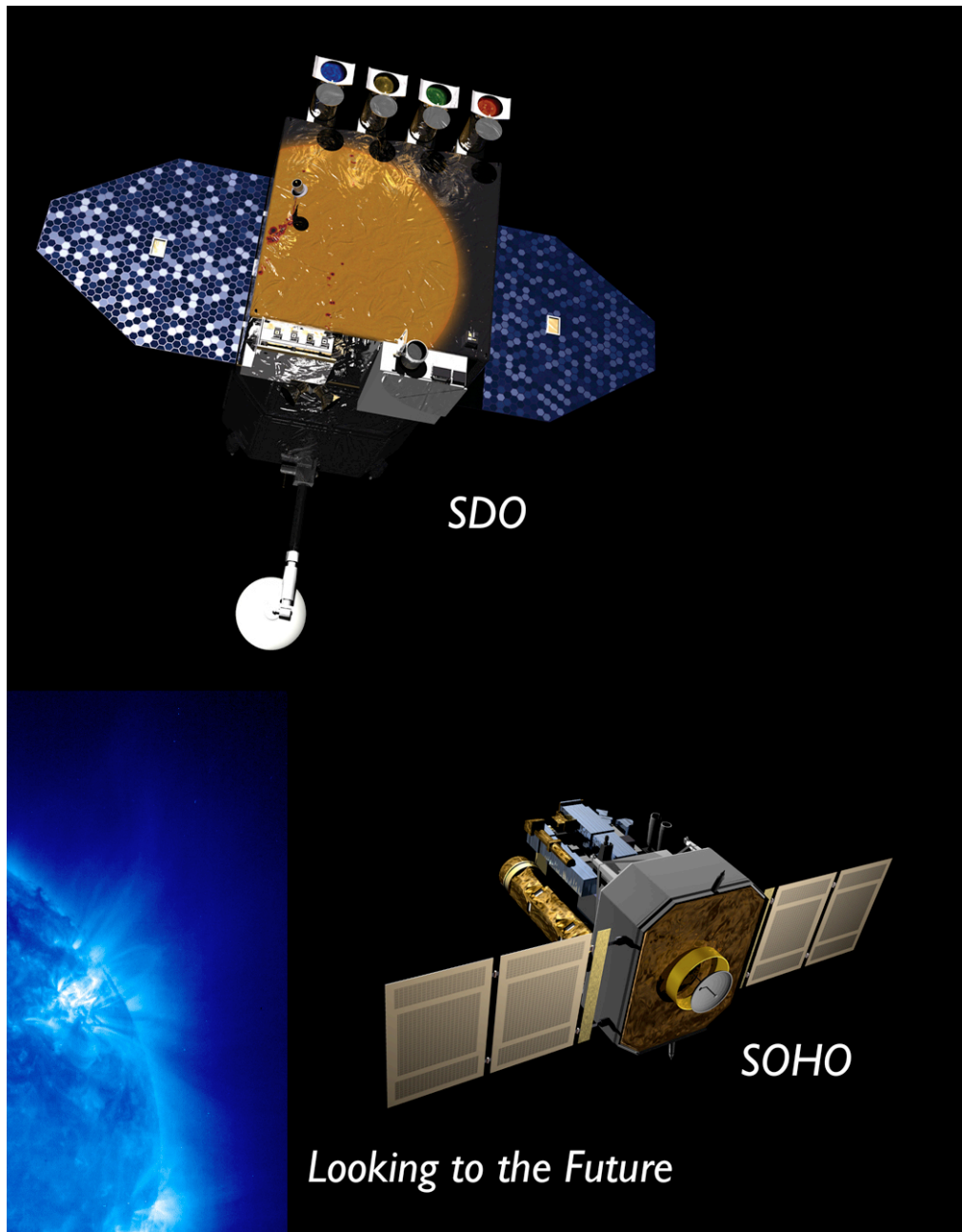
A PROPOSAL TO THE SENIOR REVIEW OF HELIOPHYSICS OPERATING MISSIONS, 2010 MARCH.

Table of Contents

Solar and Heliospheric Observatory (SOHO)

Presenters: J.B. Gurman, US Project Scientist for *SOHO*; B. Fleck (ESA; observer)

I. Executive Summary

This is the sixth Senior Review proposal from *SOHO*, but we are not requesting an extension of the mission that has led to so many exciting discoveries and so much deeper understanding of the Sun and heliosphere, from the deep solar interior to the interstellar medium. Instead, we propose here a dramatically descoped mission that nevertheless fulfills the requirement of the Living With a Star program's Solar Dynamics Observatory (SDO) mission for a white-light coronagraph to provide a Sun-earth line view of both the evolution of and transient events in the solar corona.

In the next section of this proposal (*Section II*), we summarize the widespread use and easy accessibility of *SOHO* data.

In *Section III*, we discuss a few of the many insights into the physics of the Sun, heliosphere, and beyond from the analysis of *SOHO* observations published since early 2008, when our last senior review proposal was submitted. At the beginning of each highlight we note the Research Focus Areas of the current Heliophysics Roadmap to which it is relevant.

Section IV describes the very different mission – the *SOHO* "Bogart" mission – to which we will transition this year. *Section V*, in turn, describes the technical and budget constraints of this new mission, and in particular addresses the issues of increased risk we must confront in order to operate the great observatory of the Heliophysics System Observatory for the last 14 years on a SMEX budget. Just as Humphrey Bogart regularly reduced cigarettes to the last nubbin, we propose to use *SOHO* capabilities throughout the nominal SDO mission lifetime to meet the SDO requirement for earth-Sun line coronagraphy. For virtually no operational or resource overhead, SOHO will continue to be able to provide total solar irradiance, low-frequency global solar oscillation, energetic particle, and EUV spectroscopy. For only slightly more, we can also provide UV coronagraphic spectroscopy and solar wind *in situ* plasma measurements.

Appendices describe our necessarily extremely circumscribed education and pubic outreach activities (*A*), legacy mission archive plan (*B*), publication record (*C*), and spacecraft and instrument status (*D*), as well as listing Heliophysics Roadmap Research Focus Areas (*E*) and acronyms (*F*).

II. Data Accessibility

Ubiquity. SOHO enjoys a remarkable "market share" in the worldwide solar physics community: over 3,700 papers in refereed journals since launch (not counting refereed conference proceedings, which generally duplicate journal articles), representing the work of over 3,000 individual scientists. Even accounting for the number of "heliospheric" papers and authors in those numbers, it is not too much of an exaggeration to say that virtually every living solar physicist has had access to SOHO data.

Accessibility. We can assert that with confidence because all the SOHO experiments make all their data available, online, on the Web, through the SOHO archive, at PI sites, and via the Virtual Solar Observatory (VSO). A typical PI site, the EIT Web catalog, has served over 0.35 Tbyte of data in response to over 5,800 requests since 2008 January — and the EIT database was only 800 Gbyte at the end of 2009. The entire EIT data set was replicated three times on external hard drives for export to user sites in the second half of 2009. The larger MDI database, which includes several levels of computationally expensive, higher-level data products, has served over 20 Tbyte in response to nearly 10,000 online data requests in the last two years. In addition to professional access, amateurs routinely download LASCO FITS files and GIF images to search for new comets. As a result, well over half of all comets for which orbital elements have been determined (since 1761) were discovered by SOHO, over two thirds of those by amateurs accessing LASCO data via the Web. 115 of the 177 comet discoveries in the last year confirmed by the IAU were made with SOHO observations. One, comet P/2007 R5, was determined by a radio astronomy graduate student who works on comets in his spare time to be the first periodic comet discovered from SOHO observations.

Time-lapse MPEG movies of LASCO and EIT proved so popular(> 60 Gbyte/hr of downloads) in the summer of 2009 that we had to offload service of the movies to our European mirror site at ESAC: we were interfering with Mission Network traffic flow at Goddard. A new, higher bandwidth connection to the Internet should be available in the spring of 2010.

Research access. All SOHO instruments' scientific data are accessible through a single interface, http://soho.nascom.nasa.gov/data/archive/ . This searches both the general SOHO archive at the Solar Data Analysis Center (SDAC) at Goddard, and the MDI high-rate helioseismology archive at Stanford. (MDI full-disk magnetograms obtained every 96 minutes are part of the general archive, because of their usefulness for solar activity-related research.) In both archives, and at the *SOHO* mirror site at ESAC in Spain, the holdings are identical to those used by the PI teams, and are current (i.e. to within a month or two before present, to allow time for "Level-Zero" data delivery.) Partial mirrors of the SOHO archive are maintained at the Institut d'Astrophysique Spatiale (France) and the University of Torino (Italy) for faster access by European researchers. SOHO data at both the SDAC and the Stanford Helioseismology Archive were among the first data whose metadata, including browse images for EIT and MDI, became searchable via the VSO. The VSO is designed to deliver data via the original servers, so the download traffic still occurs at those sites.

Publications. The SOHO publications database can be accessed online, as can a list of refereed SOHO papers from 2008 to the present.

III. Scientific Insights from SOHO, 2008 - 2009

The following, brief descriptions of scientific insights gained from *SOHO* have been gleaned from papers published in, or recently submitted to, refereed journals since the 2008 Senior Review. Scientific insights from earlier phases of the mission were covered in the proposals to the 1997, 2001, 2003, 2006, and 2008 Senior Reviews. Each insight is labelled with the Research Focus Area(s) from the latest Heliophysics Roadmap (see Appendix C) to which it is relevant.

Total Solar Irradiance (TSI)

Explaining TSI at the recent solar minimum (H1, H3, J1). The Sun is now emerging from the prolonged minimum of 2008-2009 which was characterized by the highest number of spotless days since the minimum around 1913, and the lowest value of TSI since reliable measurements from space became available. It was 0.20 Wm^{-2} lower than during the minimum in 1996, a decrease of 24% of the typical cycle amplitude of 0.87 Wm^{-2}. This is illustrated in Figure 1(a) (updated from Fröhlich 2009) as the cycle 23 part of the PMOD composite record (see *e.g.* Fröhlich, 2006). The uncertainty of this result for cycle 23 is discussed in detail in Fröhlich (2009) and amounts to an rms sum of 0.13 Wm^{-2}. It is mainly determined by the VIRGO radiometry, but also includes a contribution of 0.05 Wm^{-2} or about 20% from the need to bridge the gap during the loss of SOHO in 1998 with data from ACRIM-II on the UARS mission. With this rather conservatively estimated uncertainty the low TSI value is still significant at the 1.5σ level. The TSI change over cycle 23 is much larger than those of other parameters for solar activity such as the sunspot number, the 10.7 cm radio flux ($F_{10.7}$) or the MgII index,which all show a change of the order of 5 %. More importantly, the UV spectral irradiance *e.g.* at the H I Lyα line changed by only 3%, compatible with the 4% change of F10.7. The difference between the long-term behavior of TSI and the UV spectral irradiance may be caused by a global temperature change, as has been suggested by Tapping *et al.* (2007), and is possibly related to long-term changes of the strength of the solar activity. From the sensitivity of TSI to changes in temperature, a change of ≈ 0.2 K during cycle 23 would be needed. The same temperature change, however, does induce at the wavelength of Ly α a change of only 1.1 %, which is smaller than the observed 3-4 %. So, part of the TSI change – perhaps a quarter – could still be due to long-term changes of surface magnetism, which is the main driver for the cycle amplitude and the UV irradiance variability.

The only measure of solar magnetism which shows a similar behavior at cycle minima is the open magnetic field on the Sun, B_R, observed at 1 AU. B_R can be determined by taking the absolute value of the daily mean of B_X from the OMNI2 dataset, which is shown in Figure 1(b). The intra-cycle variation in B_R is not similar to that in TSI, the main reason being that B_R changes sign around the maximum of the cycle (during periods of the shaded areas in Figure 1(b)). Since the northern and southern hemisphere may change at different times, there is a prolonged period during which the behavior of the B_R variability is dominated by the reversal. During solar minima, B_R is more stable and mainly determined by the polar field, which is representative of the amount of global magnetism remaining from the previous solar cycle and available for the next one. Hence, B_R is a measure of prevailing strength of the activity. The minimum values of TSI and B_R do correlate quite well as shown in Figure 1(c), and from a linear fit the TSI-B_R sensitivity can be deduced as S(B_R) = (1364.80 ± 0.34) + (0.32 ± 0.14)B_R in Wm^{-2}. With the TSI–B_R relationship and a reconstruction of the open magnetic field from geomagnetic indices (Lockwood *et al.*, 1999, Rouillard *et al.*, 2007, Svalgaard

and Cliver, 2007), TSI can be determined from $B_R \approx 1.1$ nT at the minimum of 1912-1913 to be 1365.15 Wm−2, which is 0.43 Wm−2 lower than during the minimum of 1986. During the Maunder Minimum, $B_R \approx 0.7$ nT (Wang and Sheeley, 2003) and the reconstructed TSI was 1365.02 Wm⁻² or 0.56Wm⁻² below the minimum of 1986. From ¹⁰Be data from ice cores, B_R and thus TSI can be re-constructed back some 9300 years(Steinhilber *et al*. 2009).
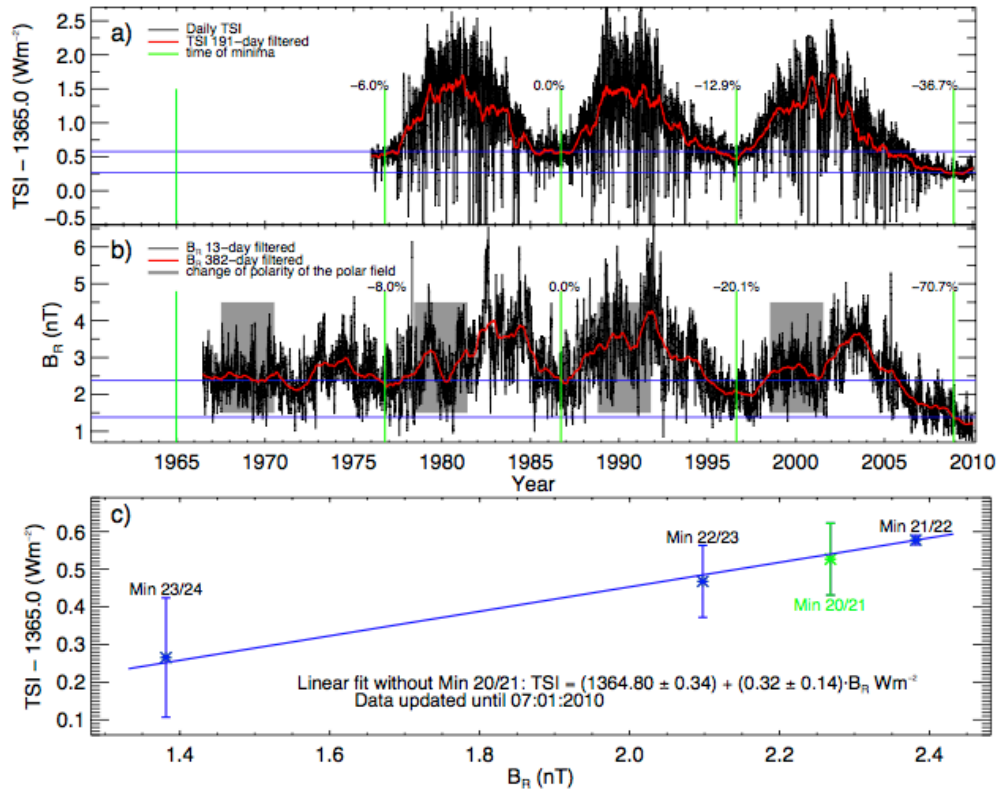
Figure 1. Comparison of TSI and open solar magnetic field B_R. Daily values of (a) TSI from SOHO VIRGO (1996-present) and earlier sources, and (b) BR at 1 AU derived from OMNI2 data. The horizontal, blue lines indicate the values at the 1986 and 2008 minima. The percentages indicate the change of the minimum values relative to the reference value in 1986. (c) The correlation between the minimum values of TSI and BRl the green point, corresponding to the minimum of 1976 - 1977, is not used in the regression. The error bars represent the estimated uncertainties over each cycle, referenced to the minimum between cycles 21 and 22.

The VIRGO TSI data have not only produced a highly reliable record during the last solar cycle, but also provided important information about irradiance variability on solar cycle and longer time scales.

Spectral Irradiance

Improving solar spectral irradiance estimates (H1, H3). SWAN full-sky images are used routinely to monitor the spatial and temporal variations of the solar illuminating flux at H Ly α. The most

striking aspect of this analysis is that it allows to reconstruct the flux distribution emitted from the far side of the Sun that is not directly visible from Earth or Earth orbit. For some time now, the SWAN team has been collaborating with two teams, one from LASP/UCAR in Boulder and one from NSO in Tucson to improve the prediction of the solar irradiance in the EUV and UV. These predictions are used to estimate the drag which affects satellites on low-earth orbits. The latest improvements on the prediction algorithm are described by Fontenla *et al.*(2009).

Heliosesimology
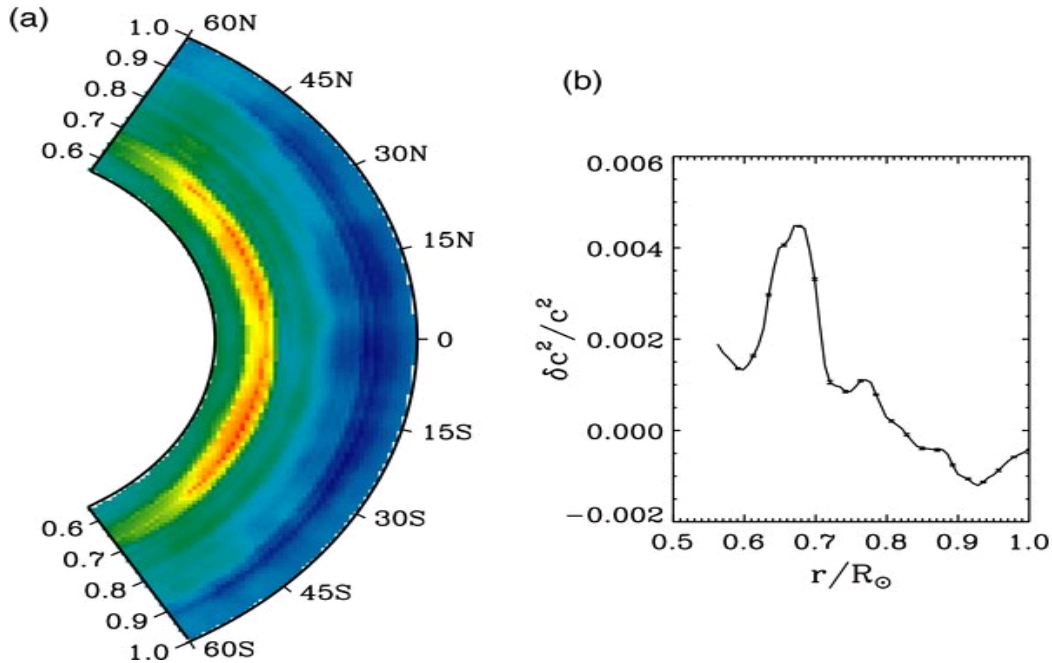
Figure 2. (a) Two-dimensional inversion results for the sound-speed perturbation from SOHO MDI measurements; the numbers 06. - 1.0 refer to fractions of a solar radius, with altitude along the outside of the longitudinally averaged plot. (b) Latitudinally averaged inversion results for SOHO MDI medium-l solar oscillation data.

Time-distance local helioseismic measurements of wave speeds near the tachocline (F4, H1, J2). Zhao *et al.*(2009) reported the first detailed study of time-distance measurements of the wave speed near the tachocline, the boundary between the Sun's convective envelope and radiative interior. Zhao and colleagues tested the method with both simulated solar data and with *SOHO* MDI data. The simulated data verified the procedure and showed that the radial and latitude resolution will be coarse, as expected for the waves that penetrate to the depth of the base of the convection zone. Analysis of MDI data, averaged over time, showed a very similar response to what is seen in long term, global averages from spherical harmonic analyses. In other words, Zhao *at al.* (2009) have demonstrated the ability to image the tachocline. Analyses of a sequence of shorter intervals showed a north-south difference that changed with the orientation of *SOHO* indicating that there is some leakage of image or filter "features" into the analysis. The MDI team plans to repeat the analysis with better removal of known instrument response functions.

5

The solar cycle viewed in torsional oscillations (H1, J1, J2). The extended *SOHO* mission has made it possible to compare the recent solar minimum and the previous one. Howe *et al.* (2009) have shown that recent *SOHO* MDI and GONG measurements of zonal flows (torsional oscillations) both show a slower equatorward drift (turquoise diagonal line in Figure 3(a), centered on 2008) of the faster-rotating zonal flow pattern than in the prior, shorter minimum. Activity tends to be centered on the poleward side of these faster bands.
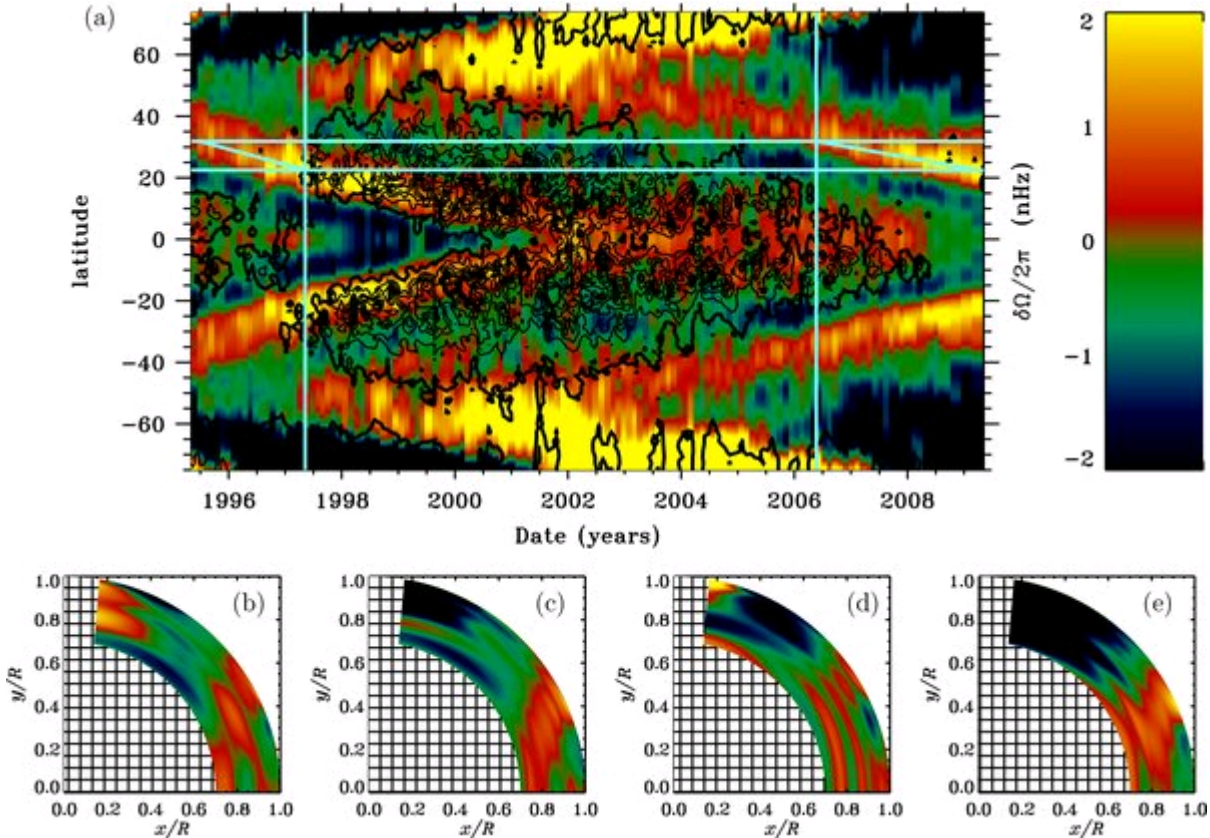
Figure 3. (a) Rotation-rate residuals at 0.99 of the solar radius from MDI and GONG. Overlaid contours show the gross longitudinal magnetic field strength from SOLIS, at 5 G intervals. The leftmost, solid, vertical turquoise line shows the date, 1997.3, at which the low-latitude flow configuration best matches that in the most recent (2009.2) data set, and rightmost vertical line the date, 2006.4, where it best matches that in the earliest data set (1996.5), while the horizontal lines show the respective location of the flow bands and the slanted lines schematically indicate the migration of the equatorward branch. The lower panels show 12-month averages of the rotation-rate residuals in the r, θ plane for epochs starting at (b) 1995.5, (c) 1996.3, (d) 2006.5, (e) 2008.2.

Daily MHD models of the corona and innermost solar wind (H1, J1, J2). Using MDI magnetograms and LASCO C2 coronagraph images as well as MLSO Mk. IV coronagraph images for the inner corona, Vásquez *et al.* (2008) demonstrated the shortcomings of MHD models of the corona and inner solar wind developed at both Stanford and the University of Michigan. As part of an effort to improve those models by including the effects of differential rotation, K. Hayashi (Stanford) is now publishing on the Web daily updates to plots of solar wind speed, number density, and magnetic field at 1.01, 2.5, and 11 solar radii. A Java applet supports visualization of these products; a static view of a snapshot from the applet is shown in Figure 4.
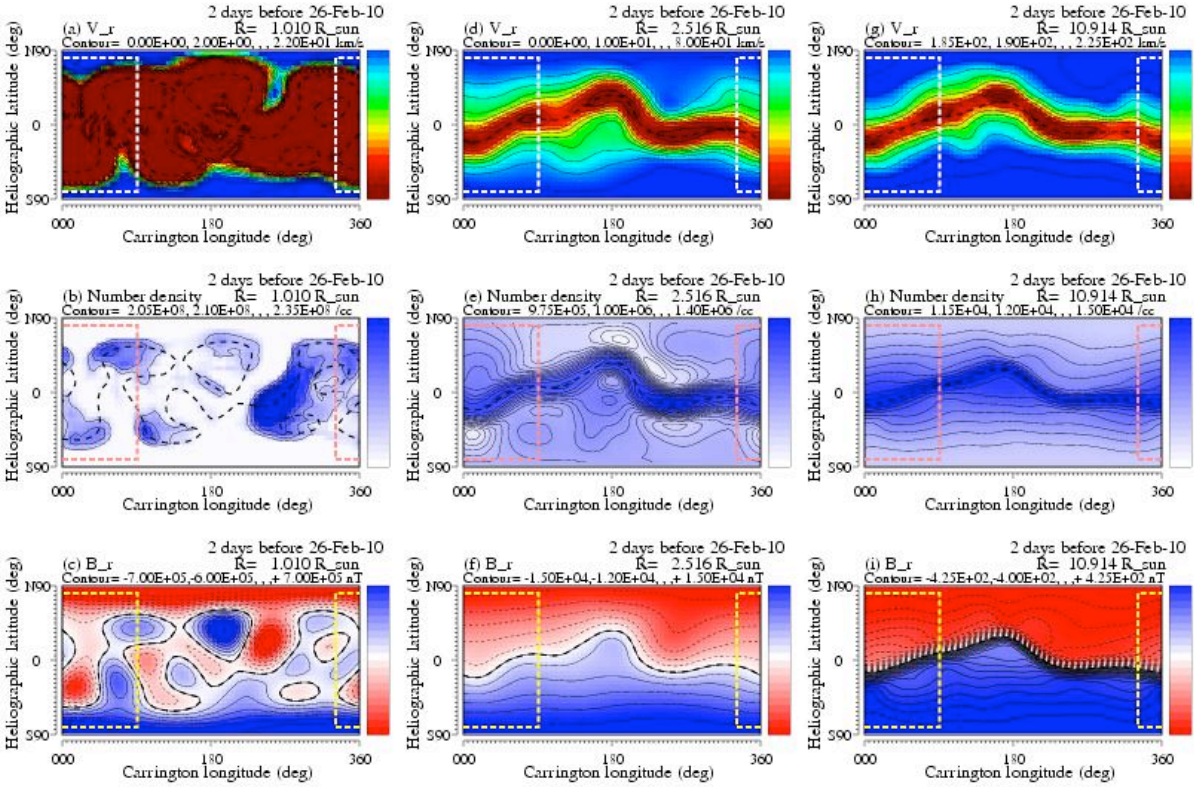
Figure 4. Snapshot of the Stanford daily MHD realtime coronal simulation, showing radial solar wind speed (top row), number density (midlle row), and radial magnetic field strength (bottom row) at (left to right) 1.01, 2.5, and 11 solar radii.

The search for solar buoyancy (g) modes reviewed (H1). Appourchaux *et al.*(2010) have reviewed the state of the art in the search for solar *g*-modes, which if detectable could be used to probe the deep solar interior. Unfortunately, after fourteen years of *SOHO* GOLF measurements, Appourchaux *et al.*conclude that "there is currently no undisputed detection of solar *g*-modes." There is, however, a possibility that measurements of the solar limb form the PICARD spacecraft or even measurements from the LISA mission may offer improved signal-to-noise.
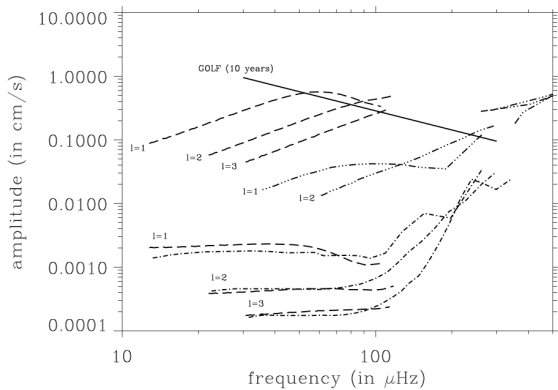
Figure 5. Estimated amplitudes of stochastically excited, solar g modes of low degree. The various dashed/dotted lines are different estimates of the amplitudes of singlet modes (single values of n, l, and m). The solid line represents the upper limit from the first ten years of SOHO GOLF measurements.

The solar atmosphere

Determining the true shape of coronal loops (H1). Alissandrakis *et al.* (2008) have shown that it is possible to find the orientation of active region loops seen against the solar disk by combining *SOHO* SUMER and CDS imaging of relatively hot plasma in the loops with measurements of Doppler shifts in flows in cooler plasma in the same loops. They found that loops in two different active regions were highly (55 - 70º) inclined to the vertical, so that the highest point in the loops above the photosphere was only on the order of a single scale height at the cooler temperatures.

Coronal loop scaling laws (H1). Fludra and Ireland (2008) used CDS measurements of four spectral lines formed at electron temperatures of 3×10^4 - 2×10^6 K in 48 active regions to test whether global scaling laws relating total EUV flux and total magnetic flux can be used to determine the coronal heating mechanism. They found that while such global scaling laws are dominated by the size of the active region and are sensitive to instrumental properties, it was possible to place a constraint on coronal heating models: $E_H \propto \phi^\gamma$, where E_H is the volumetric heating rate, ϕ is the photospheric magnetic flux density in the active region, and $0.6 < \gamma < 1.1$.

Flows and condensations in active region loops (H1). It has been known for some time that there can be a significant contribution to the TRACE 173 Å channel from transition region material. Using CDS measurements, Scott *et al.* (2008) found that bright loop tops in many TRACE images are due to overdense, O V-emitting material (characterized by electron temperatures of ~ 250,000 K), well above the height at which it is expected to be present in hydrostatic equilibrium. The cool material may be an indication that upward-propagating shock waves compress the material at the loop tops. (Note: This work was based on a Ph.D. thesis supported by a NASA Graduate Student Research Program grant.)

The solar H Lyman lines (H1). Using SUMER to study quiet Sun line profiles in an area around disk center, Tian et al. (2009) found that self-reversal (central absorption) of the emission line profiles in both lines was stronger in network cell interiors than in the bright chromospheric/ transition-region network, and that while most Ly α profiles had stronger blue than red emission peaks, the reverse was true for the less optically thick Ly β line.
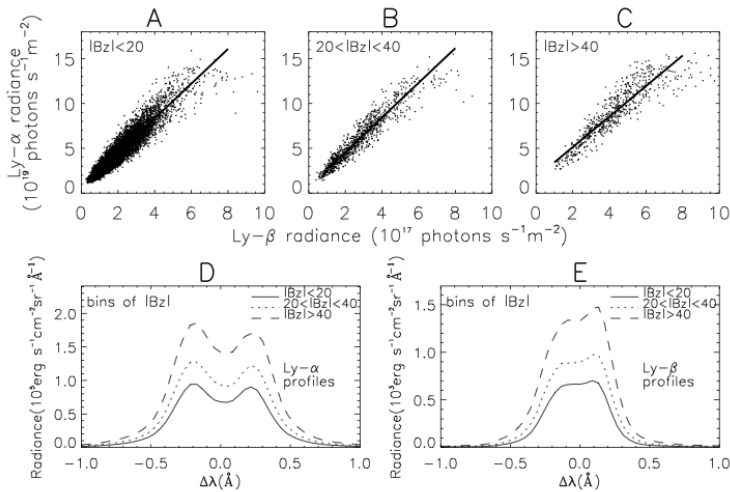
Figure 6. (A) - (C) Scatter plots of quiet Sun Ly α emission vs. Lyman β emission in ~ 1" x 1" superpixels falling three ranges of underlying, photospheric magnetic field strength measured by SOHO MDI. (D) Mean Ly α and (C) Ly β line profiles for each magnetic field strength bin. The weakest field strengths represent network cell interiors; the strongest, the network.

Coronal jets (F1, H1). Kamio *et al.* (2009) combined observations of coronal jets in coronal holes from the *Hinode* EIS and *SOHO* SUMER spectrographs with vector magnetic field measurements from the *Hinode* SOT Stokes Polarimeter to find upflows of 10 - 140 km s^{-1} originating in patches of kG, vertical magnetic field – but only when those patches adjoined areas of strong, oppositely directed magnetic field. Only then, presumably, are conditions appropriate for impulsive reconnection.

A flare/CME current sheet (F1, H1). Ciaravella and Raymond (2008) combined UVCS spectra with white light coronagraph imagery from MLSO to find the density, physical dimensions, temperature (up to 8MK) and turbulent line width of the current sheet in the CME associated with brightest soft X-ray flare (> X28) of cycle 23, on 2003 November 4. The results are consistent with the turbulent reconnection model of Lazarian and Vishniac (2000). The density structure is also consistent with Petschek reconnection provided that a substantial fraction of the reconnection inflow occurs at the height of the UVCS slit and above. The measurements of the turbulent velocities were extended to other current sheets seen by UVCS by Bemporad (2008), who found that the line width decays back to the typical coronal value over a 1-2 day timescale. Schettino *et al.* (2010) applied similar techniques to three CMEs and current sheets observed on 2003 June 2; one event was found to have even hotter plasma (10 MK) than the much larger 2003 November 4 event.
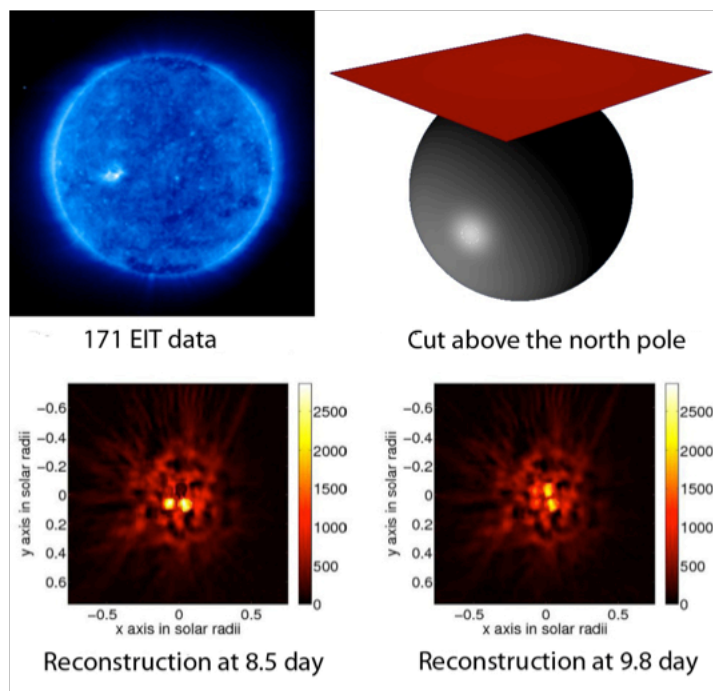
Figure 7. Temporally evolving tomographic reconstruction of polar plumes from EIT observations. The lower panels show views from above the pole of reconstructions at different times after the observations.

Tomographic reconstruction of polar plumes (F1, H1, H4). Polar plumes are raylike structures observed in polar coronal holes. They are suspected to play a role in the acceleration mechanisms of the fast solar wind, but because of their low contrast and line of sight confusion, their true nature remains elusive. Using EIT data, it was possible to reconstruct the 3D structure of polar plumes (Figure 7). Barbey *et al.* (2008) developed a time-evolving, tomographic code that is able to reconstruct at the same time the geometry and the temporal evolution of the observed structures. This is particularly important given the limited lifetime of these objects. The reconstructions suggest that plume can be more complex than simple cylindrical flux tubes.

CMEs and Type II emission (J1, J3). Afanasiev (2010) used the flux-rope CME model of Thernisien *et al.* (2006), originally developed to explain the appearance of CME's in LASCO C2 and C3 coronagraph images, to show that the fine structure in decametric type II bursts can be explained not

only by fine structure in the source, but also in the striated CME material, presumably loop structures, through which the RF emission passes on its way to the antenna.

CMEs with and without dimmings (J1, J2, J3). Reinard and Biesecker (2009) examined a sample of 90 LASCO halo CME's for which it could be determined whether coronal dimmings were detectable on disk with EIT. They found that while CMEs with dimmings occurred over a large range of propagation speeds, none of those without dimmings had speeds over 800 km s^{-1}. The bulk of the CMEs with dimmings occurred in the years around solar maximum.
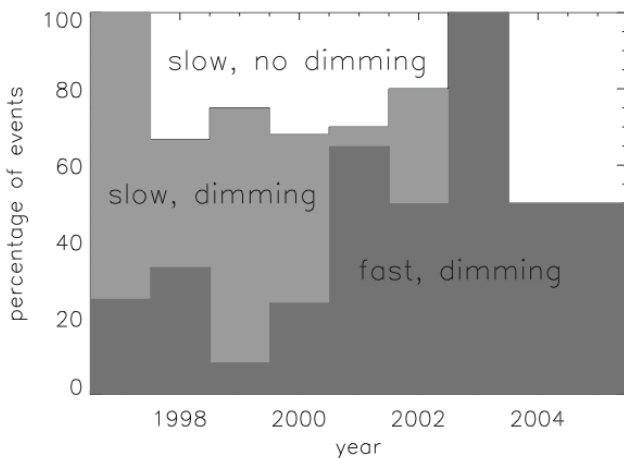
Figure 8. Solar cycle phase dependence of CME speeds and EUV coronal dimming association in Cycle 23. In 2003 and 2004, slow CMEs showed no dimming and fast CMEs were all associated with dimmings, though the picture is not so clear in during the rise to solar maximum.

The solar wind, energetic particles, and the interstellar medium

Forecasting solar radiation hazards in operational use (F2, J2, J3). It is well known that the Sun produces sudden outbursts of energetic ions. In extreme cases, particles can even be detected at sea level. The energy spectra of such particle events can be described by a power law in rigidity or energy, producing high fluxes above several tens of MeV. Above 70 MeV, protons will penetrate through the material of the spacecraft and have to be considered when calculating the radiation exposure in interplanetary space. In contrast to relativistic ions and electrons, reaching a spacecraft at Earth orbit after 11 Minutes, lower energy protons, which are the bulk of the population, need approximately one hour to travel from the Sun to 1 AU. As part of a recent trend, we attempt a rapid forecasting of bulk ion arrival at Earth by exploiting those signals that travel fast, at or near the speed of light, and so indicate particle release from the Sun.

Among the signals being investigated for operational use are relativistic electrons, relativistic ions, and plasma radiation excited by lower-energy electrons near the Sun (Dorman *et al.*, 2003; Kuwabara *et al.*, 2006, 2007; Posner, 2007, Laurenza et al., 2009). The potential for expanding Mission Operations capabilities by providing advanced warning of radiation has been acknowledged by the NASA Space Radiation Analysis Group of Johnson Space Center. The relativistic electron method (Posner, 2007, Posner *et al.* 2009) has now transitioned to operations. Electron detection at 1 AU not only provides evidence that the Sun has released charged particles into the heliosphere, but also provides a signal used to forecast the upcoming ion intensity. The method currently relies on data of the COSTEP instrument onboard *SOHO*. A forecast system called 'Relativistic Electron Alert System for Exploration' (REleASE) went online on February 7, 2008 and is distributed

worldwide from [Web servers of the University of Kiel](), COSTEP's PI institution, and of NASA GSFC [Community Coordinated Modeling Center]().

Direct measurement of the adiabatic cooling index for interstellar pickup ions in the inner heliosphere (F2, F3, J1). Interstellar neutral gas enters the inner heliosphere where it is ionized and becomes the pickup ion (PUI) population of the solar wind. It is often assumed that this population will subsequently cool adiabatically like an expanding ideal gas due to the divergent flow of the solar wind (e.g. Vasyliunas and Siscoe, 1976). Using SOHO CELIAS measurements of singly charged helium during times of perpendicular interplanetary magnetic field, Saul et al. (2009) directly measured the effective adiabatic cooling index in the inner heliosphere. Here, the cooling index γ determines the relation between the velocity, V, of a pickup ion at distance R_0 that has been injected at velocity V_{SW} at distance R, i.e. $V(R_0) = V_{SW} (R/R_0)^{\gamma}$. They use a simple adiabatic transport model of interstellar pickup helium ions, valid for the upwind region of the inner heliosphere. The time averaged velocity spectrum of helium pickup ions measured by CELIAS/CTOF is fit to this model with a single free parameter (γ) which indicates an effective cooling rate with a power-law index of $\gamma = 1.35 \pm 0.2$ (Figure 9). This effective cooling rate is not consistent with the assumption of pure magnetic cooling, i.e. the conservation of the magnetic moment. In a purely radial field, for example, this would lead to a value of $\gamma = 1$. The larger cooling rate of $\gamma = 1.35$ suggests an additional energy loss of PUI, possibly by wave - particle interactions and heating of the solar wind.

Superposed He+ Velocity Spectrum during near perpendicular IMF
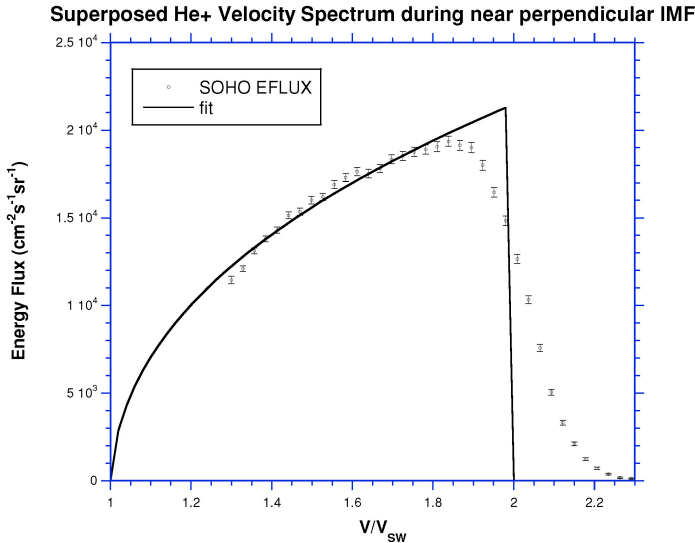
Figure 9. Solid line: Best-fit model for SOHO CELIAS CTOF measurements of pickup He+, resulting in a cooling rate of γ = 1.35±0.2. The normalized velocity is given in the spacecraft frame. The error bars represent the statistical error due to the number of counts in a given bin.

High Ionic Charge States of Iron at Suprathermal Energies: a Tracer for Local Acceleration of ICME-Related Solar Wind (H4, J1, J2, J3). Measurements of the mean ionic charge of solar energetic particles at energies of ~0.01 - 0.5 MeV/amu show a large variability, in particular for Fe. The mean Fe ionic charge states in *impulsive (Fe-rich) events* typically increase from Q_m ~11 - 15 at <100 keV/amu to 16 - 20 at ~0.5 MeV/amu (*e.g.* DiFabio *et al.*, 2008), consistent with charge stripping in a dense environment, low in the corona (Klecker *et al.*, 2007). In events related to gradual interplanetary and/or coronal shocks , the mean Fe ionic charge of Q_m ~ 9-11 at suprathermal energies (Klecker *et al.*, 2008) is usually compatible with the charge states of slow and fast solar wind. In ICME-related solar wind, by contrast, a high mean Fe ionic charge of $Q_m > 12$ and a significant fraction of charge states $Q > 15$, are often observed and, in fact, the former has been used as a reliable tracer of ICMEs (*e.g.* Wimmer-Schweingruber *et al.*, 2006). Reports on high charge states of Fe at suprathermal energies of ~ 100 keV/amu, however, are sparse.

A systematic search (Klecker *et al.* 2009) for high average Fe charge states in the suprathermal energy range of ~10 - 100 keV/amu using daily averages from the STOF/CELIAS sensor onboard *SOHO* during 2001 - 2004 showed Q_m >12 for 29 of 202 daily averages (14%). For the other 86% of the days analyzed, the mean ionic charge of Fe in the suprathermal energy range was in the range of $Q_m \sim$ 9 to 12, as usually observed at energies <0.5 MeV/amu at interplanetary shocks (Klecker *et al.*, 2008) and fast and slow solar wind. A high mean charge of Fe at suprathermal energies is generally correlated with high solar wind charge states as observed with SWICS / ACE . A high mean ionic charge of ~15 for Fe at suprathermal energies, consistent with the mean ionic charge of Fe observed at the same time in the solar wind, was observed, for example, on 2001 March 31, during a time period with unusually high solar wind density, a strong, near perpendicular interplanetary shock, and with several ICMEs and interplanetary shocks over a time period of a few days. This suggests that the rare observation of high Fe ionic charge at suprathermal energies is due to the fact that an observation is only possible if several conditions are met: (1) high Fe charge states in the seed population of an ICME, (2) a strong shock, overtaking the preceding ICME with high Fe charge states, and (3) sufficiently high solar wind density to provide adequate counting statistics.

A remarkable dual event challenges the conventional wisdom about SEP production in CMEs (F2, H1, J3). Al-Sawad *et al.* (2009) examined X1.6/2B solar flares from the same active region on 2001 October 19 and found that each was accompanied by an SEP event detected by *SOHO* ERNE. Both eruptions produced halo CMEs and shock waves observed with Wind/WAVES. Figure 10 illustrates the remarkable similarity of the events in both soft X-rays and high-energy protons at 1 AU. The time shift between the proton events is 25 min shorter than the time shift between the flares, which means that the B-event protons arrived at *SOHO* 25 minutes earlier with respect to flare B than the A-event protons did with respect to their flare. The energy spectrum of the ~10−100 MeV protons in event B was slightly softer than in event A, and the ^{4}He/p abundance ratios of the two events were different. The differences may be due to the difference in the angular distance between the Earth-connected longitude and the eruption center, which in turn is due to the solar rotation in the time between the events.
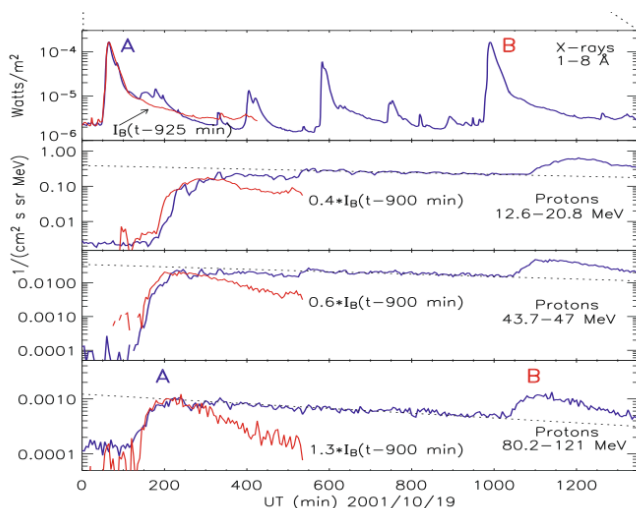
Figure 10. The soft X-ray light curves from GOES-8 and the high-energy protons observed in association with X-ray flares A and B. Red curves additionally show profiles of the event B shifted to the time of event A. An overall similarity between the events as well as some differences and time shifts are clearly seen. The proton profiles of the event B in all energy channels are similarly shifted in time, while the energy trend of the renormalization factor indicates a softer spectrum of event B compared to event A.

The current paradigm formulated by Reames (1995, 1999) suggests that energetic particles in gradual events are continuously produced at CME bow shocks during their transit to 1 AU. The interplanetary CME is assumed to

consist of a flux-rope-type structure driving ahead of it a shock wave, with a highly turbulent sheath region between the flux rope and the shock (see, *e.g.* Zurbuchen & Richardson 2006, and references therein). Particles can be accelerated to high energies in a turbulent medium at the CME bow shock, which is thought to be a moving source of SEPs in gradual events. Al-Sawad *et al.*'s event A has an extremely high p/^{4}He ratio and a prolonged intensity-time profile (Figure 11). It is associated with a halo CME and a shock wave observed near the Sun (remotely) with Wind/WAVES and (*in situ*) at 1 AU with *SOHO* CELIAS, which suggests that the shock transit speed is 650 km s^{-1} .
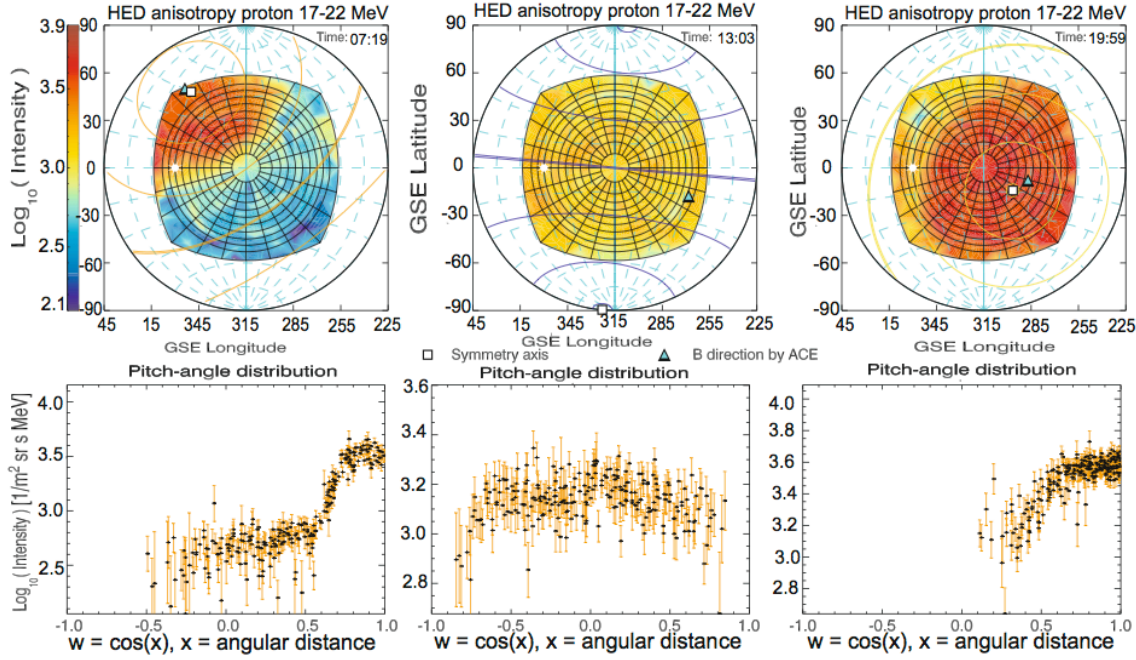
Figure 11. Angular 16.9–22.4 MeV proton flux measured by the ERNE/HED instrument at three distinct 20-min intervals indicated in the second panel of Figure 1. Upper panels show the instrument's view cone in the GSE coordinates. The direction of the Sun is indicated with a star left of the view cone center. The full circle area with coordinate lines is the hemisphere which ERNE is pointing, and the semi-rectangular borders indicate the borders of the view cone. The 241 data points, corresponding to the 241 segments of the view cone, form the pitch angle distributions in the lower panels.

Considering event A without SEP anisotropy data and without event B, a straightforward interpretation would be a gradual SEP event being continuously produced by the CME bow shock, with *SOHO* continuously staying on magnetic field lines connected to the shock. This event, however, presents severe challenges for such an interpretation. If continual acceleration at the CME bow shock on open magnetic field lines were the source of all energetic particles, as the current paradigm suggests, there should have been a continual magnetic connection to the shock driven by the first CME. The onset of the second SEP event should therefore have been observed on the magnetic field line connected to the shock of the first CME. A free penetration of the second-event particles through the shock acceleration region of the first CME, however, is inconsistent with our understanding of the turbulent sheath near the SEP-productive shock. In addition, a prolonged produc-

tion of SEPs on standard, Archimedean magnetic field lines suggests a prolonged anisotropy of the particle flux from the source, while in this event the anisotropy vanishes almost completely within 12 h, and in-creases again only at the start of the second event (B). Thus, the traditional scenario does not explain the features of the observed events.

As a plausible alternative, Al-Sawad *et al.* propose that the relatively slow shock of eruption A was SEP-productive only near the Sun, while a temporal trapping of SEPs in a possible solar wind stru-ture with a bottleneck behind the Earth's orbit (*e.g.* Bieber *et al.* 2002) resulted in extended intensity-time profiles with low values of the SEP flux anisotropy. At distances > 0.2 AU from the Sun, as suggested by the vanishing anisotropy, shock A became unable to accelerate protons to en-ergies of 17 - 22 MeV, possibly by becoming quasiparallel and surrounded by not very turbulent plasma, or even by decaying completely on the Earth-connected magnetic field lines. Thus the CME-driven compression became transparent for the >10 MeV protons and the solar-accelerated protons of the event B were able to reach *SOHO* without significant attenuation by the interplane-tary shock wave of eruption A.

Improved CME tracking using three viewpoints (F2, H1, J3). Boursier *et al.* (2009) developed CME tracking methods using the leading edge and the "center of gravity" of the observed emission and found good agreement with *e.g.* the flux rope CME model of Thernisien *et al.* (2006) when applied to four CMEs well observed by *SOHO* LASCO and both STEREO SECCHI COR-2 coronagraphs.

References

Alissandrakis, C.E., Gontikakis, C., and Dara, H.C. 2008, Solar Phys., 252, 73. DOI: 10.1007/s11207-008-9242-4

Al-Sawad, A., Saloniemi, O., Laitinen, T., and Kocharov, L. 2009, A&A, 497, L1. DOI: 10.1051/0004-6361/200811386

Appourchaux, T. et al. 2010, A&A Rev., 18, 197. DOI: 10.1007/s00159-009-0027-z

Barbey, N., Auchère, F., and Vial, J.C. 2008, Solar Phys., 248, 409

Bemporad, A. 2008, ApJ, 689, 572

Bieber, J.W. et al. 2002, ApJ, 567, 622

Boursier, Y., Lamy, P., and Llebaria, A. 2009, So-lar Phys., 256, 131. DOI: 10.1007/s11207-009-9358-1

Ciaravella, A. and Raymond, J. 2008, ApJ, 686, 1372

DiFabio, R., Guo, Z., Möbius, E., Klecker, B., Kucharek, H., MAson, G.M., and Popecki, M. 2008, ApJ, 687, 623

Dorman, L.., Pustil'nik, L., Sternlieb, A., and Zukerman, I. 2003, Adv. Space Res., 31, 847

Dröge, W., Kartavykh, Y., Klecker, B., Kovaltsov, G. 2010, ApJ, 709, 912. DOI: 10.1088/0004-637X/709/2/912

Fludra, A. and Ireland, J. 2008, A&A, 483, 609

Fontenla, J.M., Quémerais, E., González Hernández, I., Lindsey, C., and Haberreiter, M. 2009, Adv. Space. Res., 44, 457

Fröhlich, C. 2006, Space Sci. Rev., 125, 53. DOI: 10.1007/s11214-006-9046-5

Fröhlich, C. 2009, A&A, 501, L27. DOI: 10.1051/0004-6361/200912318

Howe, R., Christensen-Dalsgaard, J., Hill, F., Komm, R., Schou, J., and Thompson, M.J. 2009, ApJ, 701, L87

Kamio, S., Hara, H., Watanabe, T., and Curdt, W. 2009, A&A, 502, 345. DOI: 10.1051/0004-6361/200811125

Klassen, A., Gomez-Herrero, R., Böhm, R., Mueller-Mellin, R., Heber, B., and Wimmer-Schweingruber, R. 2008, Ann. Geophys., 26, 905

Klecker, B., Möbius, E., and Popecki, M.A. 2007, Space Science Rev. 130, 273

Klecker, B., Möbius, E. Popecki, M.A. and Kistler, L.M. 2008, Proc. 30th ICRC, Merida, Mexico, Vol. 1. p. 83

Klecker, B., Möbius, E., Popecki, M. A., et al. 2009, Proc. 31st ICRC, Lodz, Poland, 2009

Kuwabara, T. et al.2006, Space Weather, 4, S08001. DOI: 10.1029/2005SW000204

Kuwabara, T., Bieber, J. W., Clem, J., Evenson, P. and Pyle, R. 2007, Space Weather, 4 S10001,. DOI: 10.1029/2006SW000223

Laurenza, M., Cliver, E. W., Hewitt, J., Storini, M., Ling, A., Balch, C. C., and Kaiser M. L. 2009, Space Weather, Vol. 7, No. 4, S04008. DOI: 10.1029/2007SW000379

Lazarian, A. and Vishniac, E. 2000, Rev. Mex. de Astron. y Astrofís., 9, 55

Lockwood, M, Stamper, R., and Wild, M.N. 1999, Nature, 399, 437

Posner, A. 2007, Space Weather, 5, S05001. DOI: 10.1029/2006SW000268

Posner, A., Guetersloh, B., Heber, B., and Rother, O. 2009, Space Weather, 7, S05001. DOI: 10.1029/2009SW000476

Reames, D.V. 1995, Rev. Geophys., 33, 585

Reames, D.V. 1999, Space Sci. Rev., 90, 413

Reinard, A.A. and Biesecker, D.A. 2009, ApJ, 705, 914. DOI: 10.1088/0004-637X/705/1/914

Rouillard, A.P., Lockwood, M., and Finch, I. 2007, JGR, 112, A05103. DOI: 10.1029/2006JA012130

Saul, L., Wurz, P., and Kallenbach, R. 2009, ApJ, 703, 325

Schettino, G., Poletto, G., and Romoli, M. 2010, ApJ, 708, 1135. DOI: 10.1088/0004-637X/708/2/1135

Scott, J.T., Martens, P.C.H., and Cirtain, J.W. 2008, Solar Phys., 252, 293. DOI: 10.1007/s11207-008-9259-8

Steinhilber, F., Beer, J., and Fröhlich. C. 2009, GRL, 36, L19704. DOI: 10.1029/2009GL040142

Svlagaard, L. and Cliver, E.W. 2007, JGR, 112, A10111. DOI: 10.1029/2006JA012130

Tapping, K.F., Boteler, D., Charbonneau, P., Crouch, A., Manson, A., and Paquette, H. 2007, Solar Phys., 246, 309. DOI: 10.1007/s11207-007-9047-x

Thernisien, A.F.R., Howard, R.A., and Vourlidas, A. 2006, ApJ, 652, 763. DOI: 10.1086/508254

Tian, H., Curdt, W., Marsch, E., and Schühle, U. 2009, A&A, 504, 239. DOI: 10.1051/0004-6361/200811445

Vásquez, A. M., Frazin, R. A., Hayashi, K., Sokolov, I.V., Cohen, O., Manchester, W.B, Kamalabadi, F., 2008, ApJ, 682, 1328

Vasyliunas, V.M. and Siscoe, G.L. 1976, JGR,81, 1247

Wang, Y.M. and Sheeley, N.R. 2003, ApJ., 591, 1248

Wimmer-Schweingruber, R., Crooker, N.U., Balogh, A. et al. 2006, Space Sci. Rev. 123, 177

Zhao, J., Hartlep, T., Kosovichev, A. G., and Mansour, N. N. 2009, ApJ, 1150

Zurbuchen, T.H. and Richardson, I.G. 2006, Space Sci. Rev., 123, 31

IV. The SOHO Bogart Mission

SOHO is unusual in the amount of realtime contact it currently enjoys: in order to downlink the scientific telemetry from the onboard recorder and allow the Flight Operations Team (FOT) to uplink commands for the roll steering law (RSL), spacecraft clock adjustment, and command loads for instruments not operated at the Experimenters' Operations Facility (EOF), *SOHO* typically receives 6.5 hours per day of Deep Space Network (DSN) coverage. In addition, roughly eight hours per day of additional DSN time allows the use of the MDI high-rate channels, which add 160 kbps to the ~ 44 kbps (including housekeeping telemetry) that normally goes to the recorder. For a single, 60 - 90 day continuous helioseismology campaign each year, *SOHO* receives nearly continuous DSN contact and thus continuous MDI high-rate telemetry.

DSN's ability to provide such generous support to *SOHO* is predicated on the operation of 34-meter antennas at Madrid and Canberra (DSS-45 and -65), and of a 34-m antenna with different characteristics at Goldstone (DSS-27) which is dedicated to serving Heliophysics missions. The shutting down of the last 26-m antennas at other DSN stations has allowed *SOHO* engineers to change the High Gain Antenna (HGA) angle slightly to minimize the duration of telemetry "keyholes" that require 70-m support. Between the keyhole periods, it is possible to schedule continuous contact campaigns for high-rate MDI support; a final such campaign this year will assure intercalibration of local helioseismology measurements from MDI and SDO HMI.

US-supported instruments. After the completion of MDI-HMI intercalibration, *SOHO* will complete its transition to the Bogart mission. The principal purpose of the Bogart mission is the continuation of earth-Sun line coronagraph imagery from the LASCO C2 and C3 coronagraphs to support the SDO mission and the entire Heliophysics System Observatory. (White-light coronagraphy was considered a priority by the SDO Science and technology Definition Team, but had to be dropped from the payload for management reasons.) LASCO will continue to be operated by a 1.5-FTE contractor team under the direction of the US Project Scientist, as it has for the last several years. After archiving is complete this year, it will no longer be possible to support more than a minimal effort by the PI team for calibration and engineering monitoring. After a period of MDI operation in low-rate mode (5 kbps of the normal 40 kbps bandwidth to the solid state recorder), that instrument will be turned off. Likewise, EIT will be used for no more than a few, synoptic images per day (for comparing long-term response changes with that of the AIA telescopes on SDO) after a briefer period of intercalibration with SDO-AIA, to be coordinated with the TRACE mission, which will also be terminated at that time. *Note that EIT science operations of this kind incur no cost or operational risk beyond that for LASCO scientific operations, as the two instruments are commanded as one, and it is our intention to run the same LASCO/EIT synoptic program every day.*

The 2008 Senior Review recommended continued operation of the UVCS instrument, but the current funding guidelines will only permit its operation for through FY11, and then only with a generous infusion of scientific support from the PI institution, Smithsonian Astrophysical Observatory. Similarly, it will be necessary to terminate operation of the CELIAS MTOF instrument after FY11 for funding reasons as well. CELIAS SEM support will end this year, after an opportunity to intercalibrate SEM and SDO-EVE. ***If, however, we are allowed to re-phase unspent contingency from FY10 (and a much smaller amount in FY11), it should be possible to extend the operations of both UVCS and CELIAS MTOF into at least part of FY13.***

European-supported instruments. European PI teams are funded by national funding agencies. CDS, CELIAS (less MTOF), COSTEP, ERNE, GOLF, SUMER, SWAN, and VIRGO will continue to be operated, at least for the immediate future, by their PI teams. SUMER has only been operated in ~ two-week campaigns for some years, but it will be able to support coordinated observations with SDO. Aside from SUMER and CDS, which will have instrumenter workstation space in the down-sized *SOHO* science operations facility, these instruments will be operated remotely, as they have since shortly after launch.

ESA support. SOHO was rated highest among ESA Solar System missions in a Solar System Working Group meeting in 2008 October for a mission extension to 2012. The following month, the Space Science Advisory Committee, considering all scientific missions, ranked *SOHO* in the highest priority group of missions (together with HST and XMM-Newton) for an extension of ESA funding. These findings were finally confirmed by the ESA Scientific Programme Committee in 2009 October. The extension provides continues support for the ESA Project Scientist's Office, including the *SOHO* Data Coordinator at ESAC.

Until recently, highly experienced ESA and ESA contractor spacecraft engineers (one each) were located at the *SOHO* mission operations center (MOC). They have returned to Europe, but at least one will be at the MOC for all regular (four times yearly) spacecraft maneuvers, as well as being available "on-call" for anomaly resolution. The ESA *SOHO* Project Scientist will remain at Goddard for the duration of the mission.

Telemetry. Thanks to an "intermittent" recording scheme perfected by *SOHO* engineers for use during the worst parts of current telemetry "keyholes" (caused by the failure of the high gain antenna east-west drive mechanism in 2003) to preserve the helioseismology, TSI, solar wind, and when possible, coronagraph image data streams, it will be possible to reduce the effective *SOHO* telemetry bandwidth by more than a factor of three while allowing LASCO observing cadence and resolution to remain unchanged. A number of low telemetry rate but scientifically important measurements will be preserved at the cost of less than 25% additional bandwidth: GOLF (low l helioseismology and g-modes), VIRGO (TSI), SWAN (interplanetary hydrogen and solar wind anomalies), CELIAS (solar wind composition and plasma properties, absent magnetic field information; integrated solar EUV flux), UVCS (UV coronal spectroscopy), COSTEP and ERNE (energetic, charged particles, including SEP early warning).

DSN contact. The requirements for daily, realtime DSN contact will decrease significantly with the end of MDI high-rate observing. We estimate that no more than 9 - 12 hours per day of DSN contact will be necessary, compared with 16 (to as much as 24 in continuous contact campaigns) over the last 14 years.

Scientific Goals, FY11 - FY14

Observing the white-light corona from the Sun-earth line (F2, J2, J3). The principal rationale for the Heliophysics Division's continued support of *SOHO* operations is to fill the lacuna left by the dropping of coronagraphs from SDO. In conjunction with the now well-separated "side" view of

the corona provided by STEREO, *SOHO* LASCO C2 and C3 will continue to observe nearly every CME visible from the earth-Sun line. After the completion of MDI-HMI intercalibration, recovering LASCO data will have the primary priority formerly assigned to MDI. Thus, even during the depths of telemetry "keyholes" four times a year, LASCO should be able to observe continuously.

Suprathermal seed population for SEP events (F1, F2, J1, J2). A major goal of UVCS observations in the coming years will be to provide the data to detect suprathermal seed population. These particles are thought to be the source populations for energetic particles (SEPs) accelerated in CME-associated shock waves, and should be detectable as a tail above the Maxwellian thermal distribution. They can be parameterized as a Kappa distribution, and UVCS can discriminate between a thermal distribution and a Kappa distribution that would have the required number of particles. The UVCS team is therefore minimizing the use of the Ly α channel in order to have it available when the Sun becomes more active, in order to observe changes in the seed particle population and to compare them with SEP measurements by STEREO.

Basal outflow maps (J1, J3). A second UVCS goal is to provide the data for outflow velocity maps of the corona at a height of 2.4 solar radii. This will be done with month long sets of observations at a set of position angles around the West limb. The O VI intensity ratio will be combined with white light data to derive outflow speeds from the Doppler Dimming. The maps will be a Carrington rotation in length with a sampling every 2.4 days. They can be used to test MHD models of the the acceleration region of the solar wind and to compare with STEREO measurements of solar wind properties.

UV far side and H ionization rate (J1, J2, F3, H4). Most of the science activities of SWAN are based on full-sky images (H ionization rate derivation, farside imaging, UV sky illumination). Only some comet observations may require scanning a small portion of the sky with a shorter period than 24 hours. With the present values of the scan parameters (integration time of 15 seconds, scan steps of 1 degree), it takes roughly 24 hours to do a full sky image with each sensor covering half of the sky. The on-board software has been patched to do these observations automatically without the need for updating the instrument tables. In normal operations, SWAN will continue to obtain full-sky observations continuously. This observation mode does not require any commanding from the ground except at the time of maneuvers when the instrument needs to be safed before a burn, and the observation needs to be restarted after a burn.

LRO lunar darkside albedo (H4, J1). [LAMP](#) is a Far UV spectrometer on the LRO spacecraft that measures the albedo of the surface of the moon in the UV. LRO has been in orbit around the moon since 2009 June. LAMP is used to study the lunar exosphere and also looks for possible signatures of ice deposited in shadowed craters. On the dark side of the moon, the main source of photons in the UV is the interplanetary background. SWAN maps are used to compute the sky emission at Ly α and derive the surface albedo of the moon. Ice deposits are visible at Lyman α because the albedo strongly decreases where there is ice on the surface. This cooperation will continue during the whole of 2010 and into possible extensions of the LRO mission.

Continuation of long-term monitoring of the solar interior and TSI (H1, J1). GOLF measurements of low-*l* modes and VIRGO measurements of TSI will continue as longs as *SOHO* and each instrument is operational.

Longitudinal distribution of energetic particle events during solar cycle 24 (F2, H4, J3). Recent simulations of a typical impulsive event by Dröge et al. (2010) are displayed in Figure 12, showing the azimuthal distribution of electrons for a certain set of transport parameters. The low instrumental background and the appropriate time resolution of SOHO/EPHIN together with observations from the two STEREO spacecraft during future particle events expected for the rising phase of solar cycle 24 will lead to the determination of transport parameters and thus make it possible to distinguish between interplanetary transport effects and physical processes close to the Sun.
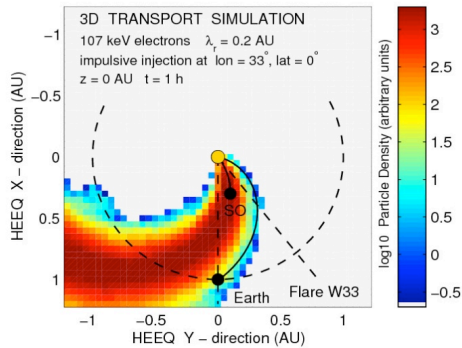
Figure 12. Distribution of 107 keV electrons in the equatorial plane, one hour after impulsive injection at a solar latitude and longitude of 0° and 33°, respectively, at a radial distance of 0.05 AU. The perpendicular mean free path scales with the particles' gyroradius.

An event of this type was detected on 2009 December 22, and was measured by not only *SOHO* EPHIN, but also by the IMPACT SEPT instrument on the STEREO Behind spacecraft, making this the first event in solar cycle 24 observed over 130° of longitude. In the next four years, EPHIN, as the only instrument measuring MeV electrons at L1, will be critical to our understanding of such events.

Improved solar wind algorithms (J2, J3). A new and improved set of algorithms for deriving solar wind parameters from the CELIAS/MTOF/Proton Monitor is undergoing final testing. This improvement will allow, for example, more stringent testing of the observed strong solar wind He/H solar cycle variation as described in the previous Senior Review, as well as detailed tracking of the expected increase in this ratio during the rising phase of the solar cycle and the consequences for the Coulomb-drag model of the extraction of minor ions into the solar wind. The real-time Proton Monitor data will also become increasingly important as we approach solar maximum. The only other available real-time data set is from ACE, which can be seriously degraded during intense energetic particle events, and from the STEREO spacecraft, which are now far from the earth-Sun line.

Energetic Neutral Atoms (F2, H4, J1). The long-term behavior of the energetic neutral atom flux in the 58 to 88 keV/n energy range from CELIAS/HSTOF is of considerable interest for comparison with the IBEX and Voyager data sets. IBEX is providing measurements of neutral atoms in the energy range up to 6 keV, not overlapping with *SOHO* CELIAS, but restricting very well potential heliospheric models. A separate issue is the time variation of the neutral atom flux measurements, *i.e.*, the comparison of the time variations as observed with IBEX to the long-term variation in the *SOHO* CELIAS data set since 1996. *In situ* Voyager data from the nose region of the heliosphere have already been used as a complementary data set to the SOHO/CELIAS neutral atom observations for the estimation of the thickness of the heliosheath.

V. Technical and Budget, FY11 - FY14

V.A The automation of SOHO operations

Starting in late 2006, in response to the budget guidelines from the previous Senior Review, the *SOHO FOT* began an in-house reengineering effort to automate *SOHO* mission operations. In the first phase of the transition from well-manned coverage of all contacts to complete automation with Observatory Engineers (OE's) on call, in 2007 September the FOT began the routine automation of all GSFC-local nighttime contacts. That followed three months of engineering trials when almost all night contacts were automated. All contacts were automated by the end of FY2009. Anomaly resolution and a restricted subset of critical spacecraft operations will continue to be carried out by the FOT; otherwise, they will construct pass plans in advance that contain all command procedures and loads. The automation software directs the commands to the existing TPOCC software, and COTS anomaly detection and notification software notifies the OE's and appropriate experiment team members (in case of an instrument anomaly). After the completion of MDI-HMI intercalibration (see section V.C, below), a major simplification will result from discontinuing daily roll steering law updates to keep the *SOHO* spacecraft Z axis aligned with the solar rotation axis. Instead, the spacecraft will be allowed to maintain its natural orientation with respect to the ecliptic. (Maintaining the spacecraft Z-axis with constant orientation with respect to the solar rotation axis was an MDI requirement; without that maintenance, LASCO images can be rectified on the ground.)

FOT compliment (FTE)	"Classic" SOHO	Current	Bogart mission
Observatory engineers	4.45	6.05	4.05
Console operators	9.90	None	None
DSN schedulers, others	7.70	1.06	0.96
Total	22.05	7.11	5.01

Table V-1. SOHO Flight Operations Team staffing before 2006 ("Classic"), after the first phase of operations automation ("Current"), and during the Bogart mission. The figures do not include partial FTE's of shared resources such as sustaining engineering and Flight Dynamics.

As shown in Table V-1, the size and skill mix of the FOT will change as well: we have eliminated the console operator positions, and all of their non-commanding functions have been replaced by the automation software.

In parallel with the automation effort, a reengineering of the EOF Core System (ECS) was carried out in FY09 and early FY10 to guarantee reliability and robustness throughout the Bogart mission. A similar reengineering effort will be carried out this year for the Data Production System (DPS). which is currently based on antiquated hardware and an outdated operating system.

V.B Risk mitigation in a fully automated scenario

We would be remiss if we did not discuss the risks we assumed in the transition to automation. Foremost among these are the possibility of inadequate notice of a critical anomaly, and failure to be able to act in time to correct a mission-threatening situation in a timely fashion. The COTS monitoring and notification software provides for full and timely FOT insight into the nature and seriousness of the anomaly. Timeliness of notification is clearly important, but fourteen years of *SOHO* operations have taught us that we never want to respond too quickly to a spacecraft anomaly; indeed, experience has shown that a series of meetings of program management, operations teams, and engineers beginning the next working day is always adequate to insure both the efficient use of onboard resources and fastest *safe* recovery of science operations. The Emergency Sun Reacquisition (ESR) mode into which the spacecraft falls in the case of serious anomalies is stable for up to 48 hours, and ground intervention at scheduled contacts (more frequent in the case of spacecraft anomalies) minimizes thruster fuel usage. With fewer instruments operational, full recovery will be faster than currently, even with less DSN contact. Both the experience of numerous missions operated by GSFC, including the ACE mission at L1, and the *SOHO* automation experience to date, demonstrate that anomaly rates actually decrease when operations are automated. Most importantly, the reduction in size of the FOT is counterbalanced by the expertise of the staff, which now consists primarily of veteran Observatory Engineers who are intimately familiar with the spacecraft and ground system.

V.C SOHO to Bogart transition

FY10 is a year of transition from the *SOHO* mission to the Bogart mission. UVCS is being operated remotely, and MDI will complete its intercalibration with HMI before being turned off. After a shorter period of intercalibration with SDO Advanced Imaging Array (AIA), EIT will also stop observing, except for two, four-wavelength "synoptic sets" per day to monitor long-term throughput changes.

At the beginning of FY11, the LASCO, MDI, CDS, and SUMER workstations and the EOF Core System (ECS) will be moved to Building 21 at GSFC, which houses the Heliophysics Division, and the *SOHO* EOF will be abandoned. The Mission Operations Center (MOC) and a facility for the non-resident PI teams' workstations, including those of UVCS, will remain in their current location in Bldg. 3.

V.E SOHO to Bogart: science team funding

With the exception of CELIAS (a foreign PI-led effort with a lead US Co-I) and UVCS, whose operations are now partially funded by the home institution (SAO), funding for US science teams will be phased out after FY10. Thereafter, LASCO will be operated by 1.5 FTE of skilled operators of the instrument who have worked under contract directly to NASA for several years, and will continue to do so in the Bogart mission. The operators will also be responsible for the maintenance and administration of the ECS, which enables near-realtime commanding between science teams' workstations on the Open IONet and the *SOHO* Command Management System (CMS) on the more secure Restricted IONet. As part of the planning for the Bogart mission, we examined whether the

ECS and CMS were necessary, and concluded that they were: the FOT uses the CMS to build command loads, and we need a secure gateway between the investigators' workstations and the CMS. The LASCO PI team engineering expertise will continue to be available, on call, if instrument anomalies occur.

MDI is the only instrument funded for data analysis in FY10; in FY11, MDI will complete its archiving. Some LASCO calibration activities will continue into FY11, but those are funded in kind at a French Co-I institution by CNES.

V.F Budget

US PI and lead CO-I teams (except for UVCS and CELIAS MTOF) are being phased out, the FOT has been reduced to a level appropriate for operating a SMEX-class mission without sacrificing expertise, and mission archiving will be completed in FY10. FY11 and after are foreseen to be a steady state, so long as *SOHO* is able to contribute to SDO and the larger Heliophysics System Observatory effort.

In FY10, we will complete the reengineering of the Data Processing System (DPS), which is likely to involve 0.50 FTE of effort. That is likely to consume part of the ~ $980K contingency in the FY10 budget. The contingency is that large specifically to deal with issues related to the transition to the Bogart mission (re-engineering efforts) and the move to Bldg. 21.

The budget figures in Table V-2 are organized differently from the ones in the Senior Review standard format (separate spreadsheet and Table V-3); they are organized by actual commitments that the US Project Scientist has to meet in order to insure the scientific success of the mission.

In FY10, there are contingencies to cover FOT overtime in case automated operations do not provide adequate response to ground station configuration issues during MDI continuous contact campaigns, including the crucial MDI-HMI intercalibration periods. Additional contingency funds cover re-engineering of science operations infrastructure that must last the five-year lifetime of SDO in order for *SOHO* to support that mission's prime phase, as well as covering some of the costs of the move to Building 21. The Heliophysics Mission Operations and Data Analysis (MO&DA) Program Executive has approved in principle the rephasing of any unused contingency funds to future fiscal years to extend the operation of UVCS and CELIAS MTOF as long as possible.

We have been informed that NASA will propose to Congress to do away with full-cost accounting for civil service labor, so the costs for civil service labor at Goddard – reduced in the Bogart mission in any case to a US Project Scientist/LASCO operations/EIT archiving scientist (0.4 FTE), a resource analyst (0.25 FTE), and a Mission Operations Director (0.25 FTE) may disappear from our actual budgets.

The "full-cost communications" line is a relatively new one, instituted by the NASA Integrated Services Network (NISN) to show full-cost accounting for the use of IONet tail circuits, Voice and

Data System (VDS) boxes used in mission operations, and related costs. We have reduced the number of VDS boxes used by *SOHO,* and will monitor efforts by SSMO to control these costs.

Category	FY10	FY11	FY12	FY13	FY14	Totals
PI teams						
MDI (Stanford)	660.0					
UVCS (SAO)	464.0	372.0	385.0	398.5	412.4	
LASCO (NRL)	125.0	50.0	50.0	50.0	50.0	
CELIAS (MTOF; UMd)	267.0	159.0	155.3	160.7	166.3	
CELIAS (SEM; USC)	107.0					
GSFC science						
LASCO ops	312.0	322.9	334.2	345.9	358.0	
Ops. coordination		0.0	0.0	0.0	0.0	
Other mission expenses	21.5	86.5	21.0	21.6	21.4	
Civil serv. science labor	68.3	72.0	75.6	80.0	84.2	
C.S. resources labor	33.1	45.0	36.6	38.7	40.8	
Institutional taxes	48.8	58.2	52.7	54.8	57.0	
Mission Operations						
C.S. mission ops. director labor	53.2	56.0	58.9	62.3	65.6	
Intercalibration campaign	300.0					
Move contingency	126.0					
Full-cost comms.	12.1	12.5	12.8	13.2	13.6	
FOT + FDF	1416.7	1416.2	1459.2	1458.8	1458.4	
Total	**4014.7**	**2650.3**	**2641.3**	**2684.4**	**2727.7**	**14718.4**
Total with instrument terminations	**4014.7**	**2650.3**	**2101.0**	**2125.2**	**2149.0**	
Guidelines	**5000.0**	**2682.0**	**2101.0**	**2200.0**	**2289.0**	**14272.0**

Table V-2. The SOHO and Bogart budget as the project scientist sees it every day. All figures in $K.

*Note that the totals for FY10 and FY 11 are **below** the guidelines, but that to remain within annual guidelines, we would have to terminate UVCS and CELIAS MTOF operations (grey boxes). Note that by rephasing unspent funds in FY10 - FY12, we should be able to keep both UVCS and CELIAS MTOF operating into FY13.*

	FY10	FY11	FY12	FY13	FY14
1. Development	0.0	0.0	0.0	0.0	0.0
2.a Space Communications	12.1	12.5	12.8	13.2	13.6
2.b Mission Services	1716.7	1416.2	1459.2	1458.8	1458.5
2.c Other Mission Operations	302.6	186.2	195.0	205.7	216.2
3. Science Center Functions	1938.8	1040.7	979.9	1011.7	1044.5
4. Science Data Analysis	50.0	0.0	0.0	0.0	0.0
5. E/PO	0.0	0.0	0.0	0.0	0.0
Totals	**4020.2**	**2655.6**	**2646.9**	**2689.4**	**2732.8**
Guideline	**5000.0**	**2682.0**	**2101.0**	**2200.0**	**2289.0**

Table V-3. The SOHO and Bogart budget as required for this proposal. All figures in $K.

The SSMO management and FOT contractor team deserve full credit not only for their work on the automation of *SOHO* operations, but also for working to reduce FOT staffing dramatically while retaining crucial expertise and minimizing operational risk.

Appendix A. Education and Public Outreach

Education

SOHO educational activities have generally been carried out by the two US PI teams at major universities (MDI at Stanford and UVCS at the Harvard-Smithsonian Center for Astrophysics). Stanford's MDI budget ends with the current fiscal year (FY10), and UVCS operations have been extended past FY10 only by limiting the budget strictly to operations, and then only with the donation of fractional FTE's from the Smithsonian Institution. Thus, no formal educational activities are proposed for the Bogart mission.

Outreach

Given the dramatic new imaging and video coming from *Hinode*, STEREO, and particularly SDO in the very near future, it is only appropriate for *SOHO* to take a back seat in outreach, particularly as we prepare to be eclipsed by the awesome potential of SDO for communicating the drama of the solar atmosphere. We will continue to run *SOHO* "Hot Shot"stories when scientific news breaks, usually in conjunction with NASA and/or ESA press releases, and we will continue to fulfill every request from the media for *SOHO* material, but it is simply more appropriate for the newer solar and heliospheric missions to grab the spotlight that *SOHO* and TRACE nearly monopolized for twelve years. Since outreach activities will be driven primarily by other missions in the years covered by this proposal, therefore, we do not include them in our baseline budget, but instead plan to deal with the very low level of costs likely to be incurred out of contingency in our "other mission expenses" budget line.

Despite striking imagery from *Hinode* and STEREO, interest in the *SOHO* Website remains high, with over 240 Tbyte of traffic generated by 691 million hits in the last two years (2008 March - 2009 February) – a mean rate of over 30 Mbps. Since the transfer of the LASCO and EIT movies to the *SOHO* European mirror site, the traffic on the US site alone appears to have relaxed to ~ 50 - 60 Tbyte per year, but with similar volume shifted to the European site.

Appendix B. Legacy Mission Archive Plan

With some minor exceptions, *SOHO* active archiving is robust: level-0 or -0.5 data are publicly available within minutes to hours of their ground receipt, level-1 and higher products within a few months to a year, and documentation and calibration databases are also publicly available. The existence of multiple copies of the archive with public Internet access insures the survival of the current state of the archive, and facilities in both Europe and the US used for active archiving will serve as resident archives after the mission ends. Instrument resource Web pages direct potential users to publications, calibration information, software descriptions, and user's guides, as well as to a variety of methods for accessing the data. All *SOHO* data are accessible via the Virtual Solar Observatory.

Existing Mission Archives and Online Resources. The information on the SOHO mission, instruments, spacecraft ephemeris, attitude, the access to both the SOHO mission archive (less MDI helioseismology observations), and publications databases, as well as access to calibration and data analysis software is available both in the US (NASA/GSFC), and in Europe (ESA/ESAC). There are two Websites and two mission archives, providing independent, redundant access points, and disaster recovery for each other, one in the [US](#) and one in [Europe](#). Each SOHO instrument PI team has a Webpage with links to standardized resources, including, but not necessarily limited to: published articles in the refereed literature describing the instrument; initial results; operational constraints; data file format description; metadata; reformatting levels; algorithms for reading the data files; recommended data access and analysis software; software and databases for calibrating lower-level data products; a user's guide to the instrument and data; and PI team contact information. Links to all of these instrument resources pages can be found at the *SOHO* [instrument resources page](#). The MDI helioseismology observations, together with the relevant documentation and software, are available online at the [Solar Oscillations Investigation Website](#). All SOHO remote-sensing data, including those at Stanford, are also accessible via the [Virtual Solar Observatory](#) (VSO), through any of the multiple access methods (physical observable, data source, data provider, etc) offered by the VSO.

Available data products.

Final science data products by instrument. Files are in FITS format except where indicated. Direct access to either of the two science SOHO archives is available [online](#).

GOLF
- Uncalibrated, full time resolution data per photomultiplier channel, level-1.
- Calibrated, full time resolution data (whole Sun average Doppler velocity in m/s calibrated using three different methods).

VIRGO
- Level 1 high resolution data organized per detector.
- 1 minute cadence time series of calibrated VIRGO total solar irradiance deduced from PMO6V data (ASCII).
- 1 hour cadence time series of calibrated total solar irradiance, PMO6V and DIARAD corrected (ASCII).
- 1 day cadence time series of calibrated total solar irradiance, PMO6V and DIARAD corrected, with DIARAD IRMB level 2 data (ASCII).
- 1 minute, 1 hour, and 1 day cadence time series of all three SPM channels, calibrated (ASCII).
- LOI 12 pixel images filtered with a 2 day triangular filter (ASCII).

MDI
- Original telemetry as received by the SSSC (SFDU)
- Level-0 MDI image data, organized by Data Product Code (DPC), the onboard-generated data tags describing unique instrument configuration and observing sequence (649 different possibilities).

- Level-1.0 data which is calibrated data in units of m/s, gauss, etc., stored in datasets of (usually) hourly data organized by DPC. (332 distinct Level-1 data series).
- Level 1.4/1.5 data which are collected into datasets named by observables, which may have contributions from multiple DPCs. The 1.4 data are in telemetry order of cropped images, while the 1.5 data are two-dimensional image arrays, reformatted from level 1.4 data if necessary. The 1.5 and higher data do not require special tables to use. There are 22 Level-1.4 series and 86 level-1.5.
- Level 1.7/1.8 data which are "recalibrated," best available data created on demand from the Level-1.4/1.5 data. Level-1.8 data is the lowest processing level that is recommended for use for most science data analysis, and include the latest information on image scale, image center position, magnetic zero level, &c. Level 1.7/1.8 data are usually recalibrated on the fly at time of export. Final recalibrated values will be used when the data are ingested into a resident archive.
- Level-2 data result from further standard processing for particular purposes. These data include products such as tracked data cubes of time-series of e.g. 15-degree regions in heliographic coordinates followed for 1664 minutes. These data are used for input to "timedistance" and "ring" local helioseismology analysis. There are 120 Level-2 products.
- SHT data, Spherical Harmonic Transform data: projections of Dopplergrams onto spherical harmonics. They are used for global helioseismology. There are 45 types, with varying ranges of mode degree-l.
- LOI 12 pixel images filtered with a 2 day triangular filter (in ASCII format).

SUMER
- Uncalibrated solar spectra organized by study
- Calibration files, software, and documentation

CDS
- Uncalibrated solar spectra organized by raster
- Calibration files, software, and documentation

EIT
- Uncalibrated, full-disk (and a small number of subfield) images in 171, 195, 284, or 304 Å
- Flat fielding, degridding, calibration files, software, and documentation

UVCS
- Uncalibrated UV spectra organized per XDL detector (each file holds multiple individual exposures)
- Uncalibrated visible light data (counts from the photomultiplier tube)
- Fully calibrated UV spectral and spatial maps, organized per XDL detector
- Calibration files, calibration software, and documentation

LASCO
- Uncalibrated Fe XIV and other forbidden line C1 inner coronal images (1996 - 1998); "level 0.5"
- Uncalibrated white light, 1024x1024, coronal images grouped per coronagraph (C2 and C3); "level 0.5"
- 1024x1024 resolution white light coronal images calibrated to mean solar brightness, grouped per detector (C2 and C3); level 1

CELIAS (all files in CDF except where indicated)
- CTOF sensor rates: Start rate, Double Coincident rate, Triple Coincident rate, Solar wind speed, Proton rate, Helium rate (rates in Hz).
- CTOF matrix elements CDF CTOF high resolution matrix rates, including velocity of solar wind in m/s.
- CTOF pulse height analyzer (raw energy spectra).
- HSTOF matrix elements and high resolution matrix rates.
- MTOF sensor rates (Front SEDA rate, neutral stop rate, ion stop rate, neutral double coincidence, ion double coincidence, ion start rate, multiple front SEDA rate, multiple double coincidence rate, neutral rates).
- MTOF pulse height analyzer: Neutral/Ion identification, amplitudes, time of flight.
- MTOF time of flight spectrum (far and near sides of MCP).
- STOF high basic rate (including both STOF and HSTOF rates).
- STOF low basic rate (including both STOF and HSTOF rates).

- STOF matrix elements and high resolution matrix rates.
- STOF pulse height analyzer (raw energy spectra).
- PM radial spectra: solar wind speed and alpha (counts per 100 seconds).
- PM theta array (counts per 100 seconds) and total rates (Hz for each step).
- M radial-theta array (counts per 10 minutes).
- SEM (photon counts).
- Proton Monitor 5 minute averages (p speed, density, thermal speed, arrival direction, predicted He speed (ASCII format).
- Coronal mass ejection data (solar wind speed, kinetic velocity, density, position angle, ion densities).
- Energetic neutral hydrogen atom fluxes (55 - 80 keV, with standard deviations).
- Solar wind speed (for O, Si, Fe), and densities (O, O^{+6}, O^{+7}).
- Fe freeze-in temperatures and mean charge states.
- Fe densities by charge state (from Fe^{+7} to Fe^{+16}).
- Si densities (for Si^{+7}, Si^{+8}, Si^{+9}).
- S^{+7} density.

COSTEP (all files in ASCII format)
- Proton, deuterium, ^{3}He, ^{4}He:
    - 1 minute EPHIN counting rates given as intensities (in $1/cm^2/s/sr/MeV$ or $1/cm^2/s/sr/MeV/nucleon$; 3 energy bands).
    - 1 minute EPHIN pulse height analysis (energy deposits in MeV).
    - 1 minute EPHIN rate correction (in counts).
- Proton, He: 15 second LION counting rates given as intensities (in $1/cm^2/s/sr/MeV$) in 3 energy bands for protons, 1 for He).

ERNE (all files in ASCII format)
- LED onboard analyzed counting rates (proton and He intensities $1/cm^2/s/sr/MeV$, 10 energy bands).
- HED onboard analyzed counting rate (proton and He intensities $1/cm^2/s/sr/MeV$, 10 energy bands).
- LED and HED pulse height data (MeV).

SWAN
- Uncalibrated full sky Ly α synoptic maps in ecliptic coordinates (one every three days: full time resolution).
- Uncalibrated data organized per target of opportunity.
- Calibration files, software, and documentation.

All science data for all instruments except for MDI are available from the *SOHO* mission archives at GSFC and ESAC.

In addition, the following MDI science data products are served by the *SOHO* archive:
- Calibrated full solar disk 1024x1024 resolution 1 minute cadence magnetograms (Gauss).
- Calibrated full solar disk 1024x1024 resolution 96 minute cadence average magnetograms (Gauss).
- Full solar disk 1024x1024 resolution 6 hour continuum images in arbitrary intensity units.

Also, the complete set of science data products is available through the Virtual Solar Observatory.

Up to date information about the time ranges for which the science data products are available in the SOHO archive can be found on the archive Webpage.

Browse products. SOHO browse products are accessible at the [*SOHO* Website](SOHO Website). These include full solar disk 'near real time' images from EIT (171, 195, 284, and 304 Å), MDI (magnetograms and visible continuum) and LASCO (visible light C2 and C3 coronagraph images). The URL above also provides access to a wide variety of browse products at PI facilities like Sun far side imaging, proton and energetic particle monitors, recent solar activity information and solar and heliospheric forecasting.

Mission data products. Available online from the [*SOHO* ancillary data products Webpage](), these products, including documentation of their contents, are: spacecraft attitude and orbit information are available in FITS and CDF format; Time Correlation Log (onboard clock history) in ASCII; Daily Report (from Flight Operations Team) in ASCII; Command History Report in ASCII; Spacecraft Mode files in ASCII; and spacecraft monthly trending reports, including spacecraft events (in digital format but not public). The entire, raw telemetry data set of the service module and instruments, with the exception of MDI high data rate, is also available at the mission archives.

Additional science data products to be included in the final archive

- VIRGO level-2 data which include corrections for degradation (before end of 2010), including: 1-minute data of VIRGO total solar irradiance (TSI), hourly data of TSI (with records on VIRGO agreed, PMO6V and DIARAD corrected, PMO6V and DIARAD level 1.8); daily data of TSI (with records on VIRGO agreed, PMO6V and DIARAD corrected, PMO6V and DIARAD level 1.8); 1-minute, hourly and daily values of the 3 SPM channels; and LOI data high-pass filtered with a 2-day triangular filter.
- SUMER calibrated data (decompressed, reversed, geometrically corrected, flat-fielded using standard software tools).
- CDS calibrated level-1 data in physical units. The calibration of the whole dataset had been completed already in February 2010. An improved calibration was developed in 2009 Autumn, and it will be used in the final calibrated dataset, which will be produced by June 2010.
- EIT level-1 calibrated FITS files (within one year of the beginning of the 'Bogart' extended mission).
- ERNE additional data sets: the highest energy particles (HED/D3-stopped) will be included in the final HED pulse height data; new file types will be added containing LED and HED heavy particle spectra for selected periods and elements; and a new file type will be added containing HED anisotropy observations in a form of a single anisotropy index, describing the strength of the observed anisotropy, supplemented with pitch angle distributions from selected periods.

Available instrument software and documentation

All software specific to instrument teams is available from the Instrument Resource Pages on the SOHO Website ([http://soho.nascom.nasa.gov/data/archive/instruments.html]()), which follow a common format for all instruments. These at least include: Instrument/hardware description; data file descriptions for science and calibration files; suggested method for reading data; data sources; calibration software, data analysis software, reference library (User Guide, Software Notes, Software Resources), and contact information.

Some of the instrument resource pages listed above describe software that can be used with their data; most of the other remote sensing instruments have extensive SolarSoft code libraries for data reduction and analysis (cf. the SolarSoft "soho" tree). The contents of the SOHO branch of the SolarSoft tree is available online at: [http://soho.nascom.nasa.gov/solarsoft/soho/](). It should be noted that considerable parts of the SolarSoft tree for each instrument are used to "prep" (e.g. flat-field, degrid, rectify, and/or calibrate) the raw data stored in most of the current FITS files. When the fully calibrated and corrected files are available along with the level-0 data in the final archive, the various <instrument>_PREP routines will be useful only for testing alternate calibration approaches. The entire point of widely adopted, standard formats such as FITS is to allow calibrated data to be used with anyone's software, so long as it incorporates a FITS reader. In principle, CDF should allow the same facility. In practice, such generalization is only possible with good metadata; the SOHO FITS files use a standard set of keywords agreed on before launch that still form the basis for similar standards for the VSO, the STEREO mission...

Transition to Resident Archives

Data Access. Data will continue to be served via both mission archives in the US and in Europe, and the Virtual Solar Observatory (VSO). We will work with the Virtual Heliospheric Observatory to enable their service of as many heliospheric data sets directly as possible; in any case, all the SOHO data will be available via the VSO through translation of SPASE-based queries to VSO-native queries. We currently plan to provide direct access from the Virtual Energetic Particle Observatory to in-situ particle data set from CELIAS, COS-TEP and ERNE by the end of 2010.

The entire MDI data collection of about 220TB has now been migrated into the Solar Dynamics Observatory (SDO) Helioseismic and Magnetic Imager (HMI) and Atmospheric Imaging Array (AIA) Joint Science Operations Center (JSOC) Science Data Processing (SDP) activity. There are about 43,000 distinct MDI Data Storage and Distribution System series names mapping into the same number of JSOC series. Also, a proposal for virtual observatory support was selected and funded: During the spring and summer of 2010 MDI will generate dataseries into the JSOC DRMS with per-image record access with full metadata support instead of the base per-dataset access

Metadata. Most of the SOHO remote sensing data are stored in FITS files which have extensive metadata available in their headers; it is in part upon those metadata that the VSO has based its data dictionary.. The translation between SPASE and the VSO data model is an ongoing effort of the "Heliophysics Virtual Great Observatory," the consortium of virtual observatory efforts funded by the Heliophysics MO&DA program.

Long term archiving

Europe. A new ESA *SOHO* long term mission archive has been deployed at the European Science Astronomy Centre (ESAC), the site which is ESA's focal point for science operations and data archiving for the missions of ESA's Science Programme. The new archive is based on the technical infrastructure already developed by the ESAC Science Archive Team for astronomy and planetary missions, and has the capability of interfacing with the virtual observatories being deployed around the world. The science archives at ESAC are the permanent holding places for ESA's scientific data, including SOHO's, and they are, therefore, long term archives which hold their data in excess of 10 years.

US. The Heliophysics Science Data Management Policy calls for transitioning mission archives from Resident Archives to "a facility determined in collaboration with the NSSDC" when it is no longer cost effective to retain the data in the Resident Archives. The Policy also notes, however, that the SDAC has become a "center for excellence in providing multi-project, crossdisciplinary access to data and tools to support the broad range of science possible with the "Heliophysics Great Observatory." We therefore expect that the *SOHO* archive will continue to be served by the SDAC for some years after the end of the mission, while a backup copy of all data, documentation, and software is deposited in a deep archive facility to be determined in consultation with NASA Heliophysics management.

Appendix C. SOHO publication record, 2008 - 2010 March

SOHO refereed publication rates through the first few weeks of calendar year 2010 can be found in Table A-1.

Calendar Year	Refereed Journals only
1996	31
1997	125
1998	174
1999	297
2000	295
2001	210
2002	289
2003	305
2004	332
2005	330
2006	272
2007	360
2008	320
2009	321
2010 (to March 2)	47
Total	3708

Table A-1. SOHO refereed papers

Here, a "*SOHO* paper" is taken to mean any paper using *SOHO* data, or concerning models or theoretical interpretations of *SOHO* measurements.

"Market share" In the years since the launch of *SOHO*, there have been over 3,000 different authors and co-authors of *SOHO* papers in refereed journals. Since *SOHO* carries both *in situ* and remote sensing instruments, there is a large potential pool of authors. Considering just the remote

sensing instruments, there are roughly 600 members of the AAS Solar Physics Division and a roughly equal number of active solar physicists in Europe and Asia (combined). Past experience indicates that approximately 75% of those are "active," in the sense of publishing at least one refereed paper per year, so *SOHO* is clearly serving a large number of members of the heliospheric community as well.

Publication rate. Despite drastically reduced funding for scientific analysis of *SOHO* data both in the US and the countries of the European Principal Investigators over the last two years, the *SOHO* publication rate has remained healthy. Full-disk magnetograms and imagery from *SOHO* MDI and EIT, as well as the earth-Sun line coronagraphy from LASCO will continue to make *SOHO* a source of unique data until SDO begins observing regularly – and in the case of LASCO, throughout the SDO mission.

We are convinced that this success is based on the open and convenient accessibility of *SOHO* data and analysis software. Only a data policy of this type is likely to draw in the widest possible scientific community — including amateurs — to the enterprise of mining Heliophysics System Observatory data for their maximum scientific return.

Bibliography. A listing of *SOHO* publications in refereed journals for the years 2008 – 2010 is available online.

Appendix D. Spacecraft and Instrument Status, 2010 March 1

Spacecraft

- All spacecraft subsystems that survived the offpointing of 1998 are still operational, except for the east-west High Gain Antenna (HGA) gimbal mechanism
- The solar arrays, with two of the eight sets of sub-arrays shunted, still supply 79.48% of the at-launch power, with adequate margin for all loads
- 117 kg of hydrazine remains in the tank, sufficient for several hundreds of years of maneuvers

GOLF

- Operating nominally, with data continuity ~98% out` *SOHO* 1998-1999 "vacation" periods, including no losses during telemetry "keyholes"
- Overall throughput down by a factor of <7 since launch, but:
    - largest noise source is the Sun itself, so negligible adverse effect over most of the frequency range, including that in which the *g*-modes are expected
    - significant reduction in signal to total noise ratio in a region around 1 mHz
- No reason to doubt that GOLF can continue to function in its present mode for several years
    - Complete redundant channel still available, though unused since initial, on-orbit commissioning

VIRGO

- All VIRGO instruments (the two types of radiometers: PMO6V and DIARAD, the filter radiometers SPM, and the luminosity oscillation imager LOI), are fully operational and performing properly. The degradation of the SPM red, green and blue channels has decreased the initial sensitivity to about 75, 26 and 8 %, respectively. The corresponding rates have changed from 220, 460 and 660 ppm/day in 1996 to 65, 75 and 40 ppm/day in 2009. The blue channel is therefore still sufficiently sensitive to provide reliable data with an instrumental signal-to-noise ratio of about 10 in the 5-minute range. The radiometers PMO6V and DIARAD show a total change of sensitivity of 4200 and 570 ppm, respectively. This can be accurately corrected with an uncertainty of less than 100 ppm over the past 13 years; hence the radiometry is also accurate enough to guarantee reliable TSI values into the future.

MDI

- ~90,000,000 images; after on-board computations, ~15,000,000 raw data images downlinked
- Expected degradation in total light throughput due to changes in the front window; compensated *via* increased exposure time.
    - mean annual degradation: 4%, appears constant
- Electronics anomaly in 2009 was corrected by instrument reboot at the end of the *SOHO* keyhole
- The drift in central wavelength of the Michelson's has nearly stopped

- The drift in best focus position has moved the nominal focus setting back almost to the design point. Shortly after launch it was at the limit of the adjustment range.
    - This drift has also slowed
- In summary, no known limit to MDI's useful life

SUMER

- Pointing mechanism is once again losing steps, so the team will use hardware encoders more frequently to confirm actual positions. Rasters will still be possible, but not "movies" (repeated rasters).
- Detector A can only be operated with reduced spatial resolution (MCP anode electronics degradation); an investigation of the problem in the address decoding electronics has shown that the effect is temperature dependent. Mitigation by operating at higher temperatures is, however, only partial and not a permanent solution. Consequently, the A-detector is no longer used.
- Detector B suffered a dramatic, apparently irreversible loss of gain in its central, KBr coated section. The team believes the detector can be stabilized by operating at a lower high voltage level, but the "attenuator" sections at the outer edges of the detector should still be fully usable, as will the center of the detector for previously avoided, bright lines.

CDS

- GIS nominal; no recalibration or changes to high voltages have been necessary in the past 3 years.
- NIS nominal; microchannel plate current anomaly in 2005 July appears to have been self-healed after a series of tests and is being used for regular observations again; sensitivity in short wavelength channel 40 - 80% of pre-launch levels; expect drop to no worse than 20 - 60% if CDS is operated throughout the Bogart mission
- Electronics nominal; trending shows no aging of components
- Mechanisms: Some 'stickyness' when rastering the GIS slits necessitated a small restriction on the range of movements. This has now been compensated for by improved ground planning software that moves the allowed range of movements to outside of the restricted area. This issue no longer impacts on science. All other mechanisms continue to operate nominally.
- Thermal: As with all other components of *SOHO*, the sunward side of CDS shows a secular increase in temperature, but analysis of the science data shows that the NIS wavelength calibration remains within tolerances.
- Onboard software: No issues

EIT

- EIT is nominal
- [Instrument throughput](#) decrease stopped and reversed since 2003.
    - Reversal due to long bakeouts occasioned by telemetry keyholes
    - CCE loss can be tracked accurately with calibration lamp images
    - Degradation now understood and modeled
    - Present exposure times range from 12 s (195 Å) to 2 m (284 Å): lots of latitude left
    - Current throughput at 195 Å is comparable to that in mid-1999

UVCS

- Both UVCS detectors are affected by an analog-to-digital converter (ADC) issue that shifts counts in some row and column groups. Regions of the detector can be selected to avoid this problem in the spectral direction. After a correction to the spatial direction based on a detector background measurement, the spatial direction can be binned to eliminate the problem. After binning, 25% of the spatial area retains its original spatial resolution and 75% has a spatial bin size of 7.3 arcminutes, which is appropriate for observations of large structures (e.g., coronal holes) and suprathermal seed particle populations. The Ly α detector retains its original pulse height distribution and sensitivity over its entire photosensitive area, and the OVI detector retains its original pulse height distribution over 60% of its area. It has been decided not to operate the Ly α detector between 1 October and 1 April due to concerns about the high voltage current that increases during this period due to the increased temperature near SOHO orbital perihelion.
- Radiometry: The degradation of the responsivities varies with the largest deterioration at the lowest observed heights. For 2.0 R_{Sun}, the OVI channel responsivity is degrading at 11% per year from 1998 to 2005, gradually decreasing to about 7 % per year in 2009. Degradation is tracked using star observations and coronal vignetting scans.
- Visible light detector: Experienced an anomaly in its housekeeping telemetry system and was turned off in 2004 April. Since its principal function of verifying the LASCO electron density measurements and co-registration has been accomplished, the risk of further operation is not justified.
- Mechanisms: All mechanisms continue to behave nominally except for the Ly α grating drive, which is slow to respond when commanded; has not prevented this channel from being used for high priority science.

LASCO

- Thernisien *et al.* (2005) have performed a detailed analysis of the intensity of a set of about 50 moderately bright stars that transited through the C3 field of view
  - These 50 stars generated about 5000 observations during the lower cadence in the first three years of *SOHO* operations and about 15000 observations thereafter
  - All stars have spectra well known from 13-color photometry
  - Using these stellar spectra as standards and the observed LASCO count rates, derived the photometric calibration factors of the C3 coronagraph for all five color filters with an absolute precision of ~7%
  - Decrease in the instrument sensitivity found to be only ~3.5% over the 8 years studied or < 0.5% per year
- C2 response changes similar
- The Fabry Pérot interferometer in the C1 coronagraph did not survive the extreme cold the instrument experienced (-80C) during the 1998 *SOHO* offpointing

CELIAS

- MTOF/PM, STOF/HSTOF, SEM nominal
  - MTOF, PM efficiency degradation of 2 (Fe) to 5 (H); still extremely high S/N
  - STOF performance stable, MC degradation compensated for by increase in HV

- SEM exhibits a very slow rate of throughput degradation, consistent with a model established in 2000.
- CTOF impaired since 1996 October (HV power supply hardware failure)

COSTEP

COSTEP consists of two sensors, the Low-Energy Ion and Electron Instrument (LION), and the Electron, Proton, and Helium Instrument (EPHIN). Both instruments have suffered some degradation but continue to generate valuable scientific data and fulfill their scientific goals.

- LION: Unexpectedly high noise level in the LION detectors since shortly after launch have resulted in the loss of the lowest energy channels (< 80 keV). In the course of the mission, three of the four LION sensor heads developed disturbances, some of which can be mitigated by careful data analysis. The disturbed periods are well documented in the level-2 data specification document. As of 2009 December one LION sensor head is still functioning nominally, one has a high background, one has a moderate background and is still useful during energetic particle events, and one is no longer functional.

- EPHIN: Detector E of the EPHIN instrument showed steadily increasing noise levels throughout 1996, and had to be switched off (on 1996 October 31) to guarantee reliable measurements with the instrument. By changing the instrument configuration, the EPHIN measurements can still be achieved with slightly degraded energy resolution in a limited energy range (3-10 MeV for electrons and 25-41 MeV/n for ions). Since 2008 January, the front detector A has shown elevated noise levels correlated with heliocentric distance; this indicates that the secular heating of the front of the spacecraft has finally produced an effect after 12 years. No significant performance degradation is seen in this detector, however, and the scientific goals of EPHIN can still be achieved.

ERNE

- Secular increase in temperatures at front of spacecraft has caused increased detector leakage currents. Including radiation effects, the increase during the last five years has been roughly 20 %yr^{-1}.

- One of the detector channels of the topmost ERNE/HED detector layer malfunctioned on 2000 November 21. Updated onboard software accounts for this issue: the geometrical acceptance (view cone) of the detector is unaffected, as is the measurement of the heavy nuclei (Carbon and heavier). Also the light nuclei are unaffected up to an energy of ~ 20 MeV/n. Between 20 MeV/n and 120 MeV/n (maximum energy measured by ERNE), both the coordinate and energy values of the affected detector become increasingly unreliable. This, however, has no effect on particle identification and produces only marginal statistical fluctuation on the total energy of these particles that deposit most of their energies in the lower detector layers.

- One of the detector bias voltages of the nominal bias source failed in 2009 September. After switching to the redundant bias source, operations continued normally.

SWAN

- Instrument status unchanged since 2001

- o All four motors nominal
- o +Z hydrogen absorption cell nominal; -Z cell empty: no absorption when activated (loss occurred in 2001)
- o Both sensors calibrated using HST STIS reference spectra: +Z sensor response constant since 1998 (outside of adjustments for high voltage [HV] setting), -Z sensor response shows decline of ~ 10% per year. HV setting changed to compensate as much as possible

Appendix E. Research Focus Areas, NASA Heliophysics Roadmap, 2009 - 2030

Research Focus Areas

F1 Magnetic reconnection

F2 Particle acceleration and transport

F3 Ion-neutral interactions

F4 Creation and variability of magnetic dynamos

Open the Frontier to Space Environmental Prediction

The Sun, our solar system, and the universe consist primarily of plasma. Plasmas are more complex than solids, liquids, and gases because the motions of electrons and ions produce both electric and magnetic fields. The electric fields accelerate particles, sometimes to very high energies, and the magnetic fields guide their motions. This results in a rich set of interacting physical processes, including intricate exchanges with the neutral gas in planetary atmospheres.

Although physicists know the laws governing the interaction of electrically charged particles, the collective behavior of the plasma state leads to complex and often surprising physical phenomena. As the foundation for our long-term research program, we will develop a comprehensive scientific understanding of the fundamental physical processes that control our space environment.

The processes of interest occur in many locations, though with vastly different magnitudes of energy, size, and time. By quantitatively examining similar phenomena occurring in different regimes with a variety of techniques, we can identify the important controlling mechanisms and rigorously test our developing knowledge. Both remote sensing and in situ observations will be utilized to provide the complementary three-dimensional, large-scale perspective and the detailed small-scale microphysics view necessary to see the complete picture.

Research Focus Areas

H1 Causes and evolution of solar activity

H2 Earth's magnetosphere, ionosphere, and upper atmosphere

H3 Role of the Sun in driving change in the Earth's atmosphere

H4 Apply our knowledge to understand other regions

Understand the Nature of Our Home in Space

Humankind does not live in isolation; we are intimately coupled with the space environment through our technological needs, the solar system bodies we plan to explore, and ultimately the fate of our Earth itself. We regularly experience how variability in the near-Earth space environment affects the activities that underpin our society. We are living with a star.

We plan to better understand our place in the solar system by investigating the interaction of the space environment with the Earth and the effect of this interaction on humankind. We plan to characterize and develop a knowledge of the impact of the space environment on our planet, technology, and society. Our goal is to understand the web of linked physical processes connecting Earth with the space environment.

Even a casual scan of the solar system is sufficient to discover that habitability, particularly for humankind, requires a rare confluence of many factors. At least some of these factors, especially the role of magnetic fields in shielding planetary atmospheres, are subjects of immense interest to heliophysics. Lessons learned in the study of planetary environments can be applied to our home on Earth, and vise versa, the study of our own atmosphere supports the exploration of other planets.

Research Focus Areas

J1 Variability, extremes, and boundary conditions

J2 Capability to predict the origin, onset, and level of solar activity

J3 Capability to predict the propagation and evolution of solar disturbances

J4 Effects on and within planetary environments

Safeguard the Journey of Exploration

NASA's robotic spacecraft continue to explore the Earth's neighborhood and other targets in the heliosphere. Humans are expected once again to venture onto the surface of the Moon and one day onto the surface of Mars. This exploration brings challenges and hazards. We plan to help safeguard these space journeys by developing predictive and forecasting strategies for space environmental hazards.

This work will aid in the optimization of habitats, spacecraft, and instrumentation, and for planning mission operation scenarios, ultimately increasing mission productivity. We will analyze the complex influence of the Sun and the space environment, from origin to the destination, on critical conditions at and in the vicinity of human and robotic spacecraft. Collaborations between heliophysics scientists and those preparing for human and robotic exploration will be fostered through interdisciplinary research programs and the common use of NASA research assets in space.

Appendix F. Acronyms

ACE	Advanced Composition Explorer
AIA	Advanced Imaging Array (SDO)
CDS	Coronal Diagnostic Spectrometer
CELIAS	Charge, Element, and Isotope Analysis System
CIR	Corotating interaction region
CISM	Center for Integrated Space Weather Modeling (NSF supported)
CME	Coronal mass ejection
CMS	Command Management System
COSTEP	Comprehensive Suprathermal and Energetic Particle Analyzer
COTS	Commercial, off the shelf
CTOF	Charge Time-Of-Flight sensor of CELIAS
DIARAD	DIfferential Absolute RADiometer (active cavity radiometer) component of VIRGO
DSN	Deep Space Network
EAF	Experimenters' Analysis Facility
ECS	EOF Core System
EIS	Extreme ultraviolet Imaging Spectrograph
EIT	Extreme ultraviolet Imaging Telescope
ENA	Energetic neutral atom
EPHIN	Electron, Proton, and Helium INstrument (part of COSTEP)
ERNE	Energetic and Relativistic Nuclei and Electron experiment
ESAC	European Space Astronomy Centre (ESA)
EOF	Experimenters' Operations Facility
ESA	European Space Agency
EUV	Extreme ultraviolet
EVE	Extreme ultraviolet Variability Experiment (SDO)
FDF	Flight Dynamics Facility
FOT	Flight Operations Team
FTE	Full time equivalent (one person's work in one year)
FY	Fiscal year
GIS	Grazing Incidence Spectrograph of CDS
GOLF	Global Oscillations at Low Frequencies
GONG	Global Oscillation Network Group
HMI	Helioseismic and Magnetic Imager (SDO)
HSO	Heliophysics System Observatory
HST	Hubble Space Telescope
ICME	Interplanetary coronal mass ejection
IONet	Internet Operational Network (NASA)
IP	Interplanetary
L1	First Lagrangian libration point
LASCO	Large-Angle and Spectrometric Coronagraph
LOI	Luminosity Oscillations Imager component of VIRGO
LRO	Lunar Reconnaissance Orbiter
MDI	Michelson Doppler Imager
MO&DA	Mission Operations and Data Analysis
MTF	Modulation transfer function
MTOF	Mass Time-of-Flight mass spectrometer of CELIAS
NIS	Normal Incidence Spectrograph of CDS

NSSDC	National Space Science Data Center
OE	Observatory Engineer
PFSS	Potential-field source surface
PM	Proton Monitor of CELIAS MTOF
PM06	Twin-cavity radiometer component of VIRGO
SAO	Smithsonian Astrophysical Observatory
SDO	Solar Dynamics Observatory
SEM	Solar EUV monitor of CELIAS
SEP	Solar Energetic Particle
SOHO	Solar and Heliospheric Observatory
SOI	Solar Oscillations Investigation
SOT	Solar Optical Telescope
SMEX	Small Explorer
SPM	Spectral irradiance monitor component of VIRGO
STEREO	Solar TErrestrial RElations Observatory
STIS	Space Telescope Imaging Spectrograph
STOF	Suprathermal Time-of-Flight ion telescope, part of CELIAS
SUMER	Solar Ultraviolet Measurements of Emitted Radiation (UV spectrometer)
TRACE	TRansition Region And Coronal Explorer
SWAN	Solar Wind Anisotropies
UVCS	Ultraviolet Coronagraph Spectrometer
VIRGO	Variability of Solar Irradiance and Gravity Oscillations
VSO	Virtual Solar Observatory
XDL	Cross Delay Line

SOHO instrument names are in blue.